AD_____

Award Number: W81XWH-04-1-0700

TITLE: Nuclear Dynamics of BRCA1-Dependent Transcription Regulation

PRINCIPAL INVESTIGATOR: Zelton Dave Sharp, Ph.D.

CONTRACTING ORGANIZATION: University of Texas Health Sciences Cent
San Antonio TX 78229-3900

REPORT DATE: August 2006

TYPE OF REPORT: Final

PREPARED FOR: U.S. Army Medical Research and Materiel Command
Fort Detrick, Maryland 21702-5012

DISTRIBUTION STATEMENT: Approved for Public Release;
Distribution Unlimited

REPORT DOCUMENTATION PAGE

Form Approved
OMB No. 0704-0188

1. REPORT DATE *(DD-MM-YYYY)*	**2. REPORT TYPE**	**3. DATES COVERED** *(From - To)*
01/08/06	Final	15 Jul 04 – 14 Jul 06

4. TITLE AND SUBTITLE
Nuclear Dynamics of BRCA1-Dependent Transcription Regulation

5a. CONTRACT NUMBER

5b. GRANT NUMBER
W81XWH-04-1-0700

5c. PROGRAM ELEMENT NUMBER

6. AUTHOR(S)
Zelton Dave Sharp, Ph.D.

E-Mail: SHARP@UTHSCSA.EDU

5d. PROJECT NUMBER

5e. TASK NUMBER

5f. WORK UNIT NUMBER

7. PERFORMING ORGANIZATION NAME(S) AND ADDRESS(ES)
University of Texas Health Sciences Cent
San Antonio TX 78229-3900

8. PERFORMING ORGANIZATION REPORT NUMBER

9. SPONSORING / MONITORING AGENCY NAME(S) AND ADDRESS(ES)
U.S. Army Medical Research and Materiel Command
Fort Detrick, Maryland 21702-5012

10. SPONSOR/MONITOR'S ACRONYM(S)

11. SPONSOR/MONITOR'S REPORT NUMBER(S)

12. DISTRIBUTION / AVAILABILITY STATEMENT
Approved for Public Release; Distribution Unlimited

13. SUPPLEMENTARY NOTES

14. ABSTRACT
BRCA1 coordinates cellular responses to DNA damage. It functions as a co-repressor of GADD45aand estrogen-responsive transcription through interactions with a DNA-binding protein termedZBRK1. Our goal is to develop a biosensor system to visualize transcription control by ZBRK1and BRCA1 in single living and/or fixed cells. The rationale is to use integrated DNA bindingsites to obtain real time, multiplex-based data. The reportable outcomes for the period are:1) UAS and ZRE array-bearing plasmids have been constructed; 2) Transient and stable reporterexpression have been demonstrated; 3) Stable cell lines with G20, G40 and Z32 are on line forstudies; 4) Construction of fluorescent GAL4-DBD and ZBRK1 fusion protein has been achieved,and BRCA1 derivatives are in progress; 5) Development of a high throughput screening systemfor estrogen receptor activated transcription complex. When operational, these systems willdocument real time nuclear dynamics of ZBRK1/BRCA1-dependent chromatin modification systems,as cells mount transcriptional responses to genotoxins and identify BRCA1-associated proteinsthat mediate its actions.

15. SUBJECT TERMS
BRCA1; ZBRK1; Breast Cancer, Nuclear Dynamics

16. SECURITY CLASSIFICATION OF:			**17. LIMITATION OF ABSTRACT**	**18. NUMBER OF PAGES**	**19a. NAME OF RESPONSIBLE PERSON**
a. REPORT	**b. ABSTRACT**	**c. THIS PAGE**			USAMRMC
U	U	U	UU	25	**19b. TELEPHONE NUMBER** *(include area code)*

Standard Form 298 (Rev. 8-98)
Prescribed by ANSI Std. Z39.18

Table of Contents

Introduction:

Families carrying defective *breast cancer 1* (*BRCA1*) genes have a cumulative lifetime risk of breast and ovarian cancer (Hall et al., 1990; Miki et al., 1994; Wooster and Weber, 2003). BRCA1 coordinates cellular responses to DNA damage (Rosen et al., 2003; Zheng et al., 2000a). Functions attributed to BRCA1 include chromatin modification, ubiquitinylation, and transcription regulation. Regarding transcription, BRCA1 has been implicated in both activation and repression (Monteiro, 2000). One notable target is the growth arrest and DNA damage-inducible gene, GADD45 (Harkin et al., 1999; Jin et al., 2000; Li et al., 2000; MacLachlan et al., 2000; Sheikh et al., 2000), important in cell cycle arrest and apoptosis in response to cell stress (Sheikh et al., 2000; Taylor and Stark, 2001). BRCA1 functions as a co-repressor of GADD45 transcription by way of interactions with a DNA-binding protein termed zinc finger and BRCA1- interacting protein with a KRAB domain 1, ZBRK1 (Zheng et al., 2000b), a member of the Krupple-associated box-zinc finger protein (KRAB-ZFP) family of transcription repressors (Collins et al., 2001). The latest evidence indicates that ZBRK1 has a BRCA1-independent repressor function by way of its KRAB domain, and a C-terminal BRCA1-dependent repressor activity, $ZBRK1_{5-9}$ (Tan et al., 2004).

Our goal is to develop a biosensor system to visualize transcription control by ZBRK1 and BRCA1 in single living and/or fixed cells. The rationale is to use integrated DNA binding sites to obtain real time, multiplex-based data. When operational, this system would be capable of documenting real time nuclear dynamics of ZBRK1/BRCA1-dependent chromatin modification systems, as cells mount transcriptional responses to genotoxins.

Body:

Included with this report is a PowerPoint Presentation for the recent Era of Hope meeting in Philadelphia. This is provided to document the methodology and preliminary results. Also appended is a presentation by a student, Tiffany Jones, who worked on this project as a rotation student in my laboratory.

Negative findings are that expression of the GFP-Gal4DBD has not been found to localize at fluorescent foci in the nuclei of any of our G-series cell lines. The expression of ZBRK1-GFP has also not resulted in any fluorescent nuclear foci in any of the Z-series lines. We have attempted this screen in live cells, which has lower microscopic resolution than fixed cells, which we will try next.

Finally, our first attempt at securing funding to keep this project going was not successful (see attached application for an Idea Award). We are currently looking for alternative funding sources. Since this is a technology development project, there have been, as yet, no publications.

Key Research Accomplishments:

Key research accomplishments are the establishment of several cell lines (G-series and Z-series documented in the Body and appended PowerPoint files. We have also constructed a key screening reagent, GFP-GAL4-DBD, which is the green fluorescent protein fused to the DNA-binding domain of the GAL4 activator. Also, we have finished re-engineering ZBRK1-GFP fusion to a more modern enhanced green fluorescent protein.

During the extension period, we have taken this approach to a biochemical level using an array of estrogen receptor binding elements. Since BRCA1 interacts with the estrogen receptor, this may allow us to define the interacting proteins that mediate BRCA1 action. The reason for choosing ERE array over ZBRK1 is that the ERE-containing promoter/enhancer is active in an in vitro transcription system; that is it is functional and if BRCA1 will repress its activity, we will identify the proteins that mediate this response.

Reportable Outcomes:

- UAS and ZRE array-bearing plasmids have been constructed.
- Transient and stable reporter expression have been demonstrated.
- Stable lines with G20, G40 and Z32 are on line for studies.
- Construction of fluorescent GAL4-DBD and ZBRK1 and BRCA1 derivatives are underway.
- Development of a high throughput screening system for estrogen receptor activated transcription complex.

Data generated:

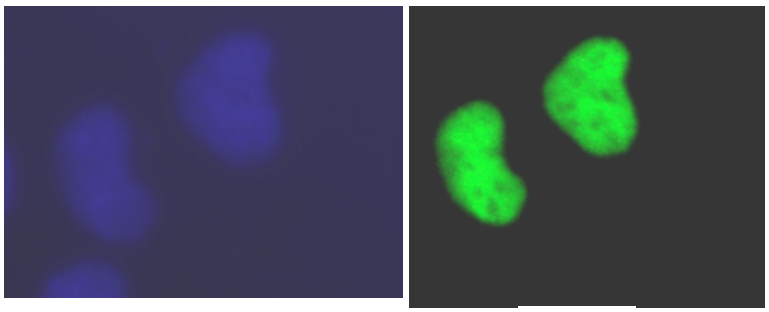

DAPI GFP

Figure 1. *ZBRK1-GFP expression plasmid.* In this experiment, a plasmid constructed by a student, Tiffany Jones, was being tested for functionality. The plasmid encodes a translational fusion of ZBRK1 and the green fluorescent protein (GFP). The purpose of constructing this plasmid is to test for binding to the Z-series clones containing multimerized ZBRK1-binding sites integrated into the chromosomes. DAPI staining identifies nuclei of three cells (one is partially in the field on the lower left) and

green fluorescence in nuclei (right) identifies two transiently transfected cells, indicating the expression plasmid is working properly.

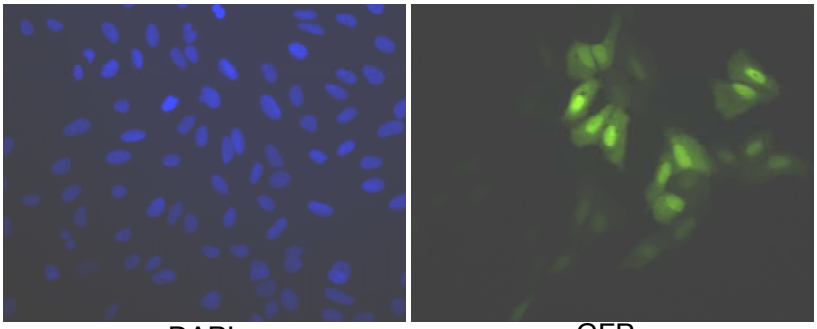

DAPI GFP

Figure 2. *GAL4-DBD-GFP expression plasmid.* In this experiment, aother plasmid constructed by a student, Tiffany Jones, was also being tested for functionality. The plasmid encodes a translational fusion of the GAL4 DNA-binding domain and the green fluorescent protein (GFP). The purpose of constructing this plasmid is to test for binding to the G-series (UAS) clones containing multimerized GAL4-binding sites integrated into the chromosomes. DAPI staining identifies nuclei of three cells (one is partially in the field on the lower left) and green fluorescence in nuclei (right) identifies two transiently transfected cells, indicating the expression plasmid is working properly. These images are taken from living cells.

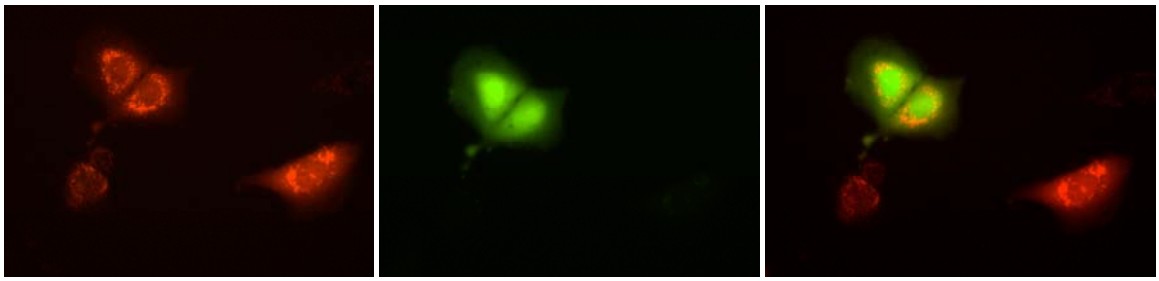

dsRed GFP Merge

Figure 3. *GAL4-DBD-GFP expression in G-series cells*. In this experiment, we conducted the first test to determine if we could visualize a nuclear focus of green fluorescence in a one clonal line stably expressing dsRED in the cytoplasm (peroxisome targeted) and presumably bearing an integrated UAS GAL4 array of binding sites. None could be detected at this resolution or upon fixation and higher resolution analysis (not shown). On the left are dsRed expressing cells, which shows peroxisome-targeted fluorescence. The panel labeled GFP shows a transiently transfected cell expressing GFP-GAL4-DBD, which is predominantly nuclear in location. The right hand panel shows a merged image.

A bidirectional expression vector that contains a cDNA encoding BRCA1 translationally fused to GFP was also completed and sequenced for verification. Transient transfections will be used to verify the functionality of this construct.

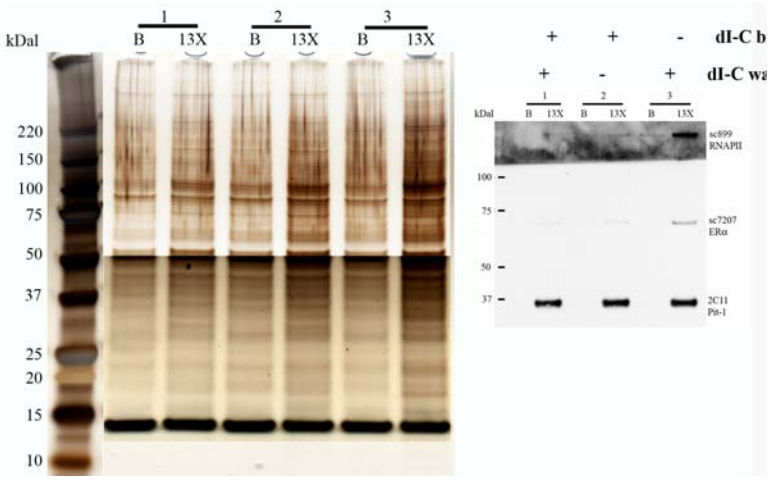

Figure 4. *Cell-free assembly of RNA polymerase II transcription complex by the estrogen receptor.* A prolactin array consisting of the promoter and enhancer plus 13 repeats of the enhancer binding sites for Pit-1 and the estrogen receptor (Sharp et al., 2006) was used in transcription complex assembly with GH3 nuclear extracts. The 13X fragments and non-specific DNA fragments (labeled 13X) were biotinylated and linked to spreptavidin DynaBeads. In reaction # 1, dI-C (as a non-specific competior) was used in both the binding buffer and wash buffer. In reaction #2, dI-C was used only in the binding reaction, and in reaction #3, dI-C was included only in the wash buffer. Lanes labeled B are DynaBeads and 13X are reactions containing Dynabeads linked with 13X array-containing DNA. The left picture shows the silver stained gel used to fractionate the proteins bound to beads. It appears to be split due to a reduction in brightness and contrast in the lower segment of gel using PhotoShop. On the right is a Western blot probed with mAB specific for Pit, antibodies for ERα and RNA polymerase II. This identified conditions #3, as optimal for assembly of ER-mediated transcription complex assembly.

The proteins assembled using this approach are being investigated by mass spectrometry by Jun Qin and Michael Mancini at the Baylor College of Medicine. They are also being used to generate at panel of monoclonal antibodies which will be screened using high content microscopy and Hela52X Prl array-containing cells (Sharp et al., 2006). Eventually, we hope to apply this technological development to identify BRCA1-associated proteins that mediate repression of the estrogen receptor.

Conclusion:

We envision our array-bearing lines as single cell biosensors for responses to DNA damage and other macromolecular trauma. For the first time it will be possible to obtain multiplex data both in real time and in high resolution fixed cell experiments. Thus, we can begin putting together a comprehensive picture of the high precision chromatin transactions involving ZBRK1 and BRCA1. This novel approach also has the potential to be adapted for other types of damage response transactions including repair and recombination. Finally, we think our cells will be extremely useful in high throughput microscopic screening that is currently coming on line in several laboratories (Perlman et

al., 2004) using image cytometry. This could be important in identifying new compounds that will either up or down regulate the genotoxic response system. Finally, we want to combine our cell based approach with a biochemical/proteomic approach to identify novel proteins in BRCA1-medicated repression of transcription, and in the process develop immunological reagents for these novel proteins.

References:

Collins, T., J.R. Stone, and A.J. Williams. 2001. All in the family: the BTB/POZ, KRAB, and SCAN domains. *Mol Cell Biol*. 21:3609-15.

Hall, J.M., M.K. Lee, B. Newman, J.E. Morrow, L.A. Anderson, B. Huey, and M.C. King. 1990. Linkage of early-onset familial breast cancer to chromosome 17q21. *Science*. 250:1684-1689.

Harkin, D.P., J.M. Bean, D. Miklos, Y.H. Song, V.B. Truong, C. Englert, F.C. Christians, L.W. Ellisen, S. Maheswaran, J.D. Oliner, and D.A. Haber. 1999. Induction of GADD45 and JNK/SAPK-dependent apoptosis following inducible expression of BRCA1. *Cell*. 97:575-86.

Jin, S., H. Zhao, F. Fan, P. Blanck, W. Fan, A.B. Colchagie, A.J. Fornace, Jr., and Q. Zhan. 2000. BRCA1 activation of the GADD45 promoter. *Oncogene*. 19:4050-7.

Li, S., N.S. Ting, L. Zheng, P.L. Chen, Y. Ziv, Y. Shiloh, E.Y. Lee, and W.H. Lee. 2000. Functional link of BRCA1 and ataxia telangiectasia gene product in DNA damage response. *Nature*. 406:210-5.

MacLachlan, T.K., K. Somasundaram, M. Sgagias, Y. Shifman, R.J. Muschel, K.H. Cowan, and W.S. El-Deiry. 2000. BRCA1 effects on the cell cycle and the DNA damage response are linked to altered gene expression. *J Biol Chem*. 275:2777-85.

Miki, Y., J. Swensen, D. Shattuck-Eidens, P.A. Futreal, K. Harshman, S. Tavtigian, Q. Liu, C. Cochran, L.M. Bennett, W. Ding, R. Bell, J. Rosenthal, C. Hussey, T. Tran, M. McClure, C. Frye, T. Hattier, R. Phelps, A. Haugen-Strano, J. Katcher, K. Yakumo, Z. Gholalmi, D. Shaffer, S. Stone, S. Bayer, C. Wray, R. Bogden, P. Dayananth, J. Ward, P. Tonin, S. Narod, P.K. Bristow, F.J. Norris, L. Helvering, P. Morrison, P. Rostek, M. Lai, J.C. Barrett, C. Lewis, S. Neuhausen, L. Cannon-Albright, D. Goldgar, R. Wiseman, A. Kamb, and M.H. Skolnick. 1994. A strong candidate for the breast and ovarian cancer susceptibility gene BRCA1. *Science*. 266:66-71.

Monteiro, A.N. 2000. BRCA1: exploring the links to transcription. *Trends Biochem Sci*. 25:469-74.

Perlman, Z.E., M.D. Slack, Y. Feng, T.J. Mitchison, L.F. Wu, and S.J. Altschuler. 2004. Multidimensional drug profiling by automated microscopy. *Science*. 306:1194-8.

Rosen, E.M., S. Fan, R.G. Pestell, and I.D. Goldberg. 2003. BRCA1 gene in breast cancer. *J Cell Physiol*. 196:19-41.

Sharp, Z.D., M.G. Mancini, C.A. Hinojos, F. Dai, V. Berno, A.T. Szafran, K.P. Smith, T.T. Lele, D.E. Ingber, and M.A. Mancini. 2006. Estrogen-receptor-{alpha} exchange and chromatin dynamics are ligand- and domain-dependent. *J Cell Sci*. 119:4101-16.

Sheikh, M.S., M.C. Hollander, and A.J. Fornance, Jr. 2000. Role of Gadd45 in apoptosis. *Biochem Pharmacol*. 59:43-5.

Tan, W., L. Zheng, W.H. Lee, and T.G. Boyer. 2004. Functional dissection of transcription factor ZBRK1 reveals zinc fingers with dual roles in DNA-binding and BRCA1-dependent transcriptional repression. *J Biol Chem*. 279:6576-87.

Taylor, W.R., and G.R. Stark. 2001. Regulation of the G2/M transition by p53. *Oncogene*. 20:1803-15.

Wooster, R., and B.L. Weber. 2003. Breast and ovarian cancer. *N Engl J Med*. 348:2339-47.

Zheng, L., S. Li, T.G. Boyer, and W.H. Lee. 2000a. Lessons learned from BRCA1 and BRCA2. *Oncogene*. 19:6159-75.

Zheng, L., H. Pan, S. Li, A. Flesken-Nikitin, P.L. Chen, T.G. Boyer, and W.H. Lee. 2000b. Sequence-specific transcriptional corepressor function for BRCA1 through a novel zinc finger protein, ZBRK1. *Mol Cell*. 6:757-68.

Estrogen-receptor-α exchange, and chromatin dynamics are ligand- and domain-dependent

Z. Dave Sharp[1,*], Maureen G. Mancini[2,*], Cruz A. Hinojos[2,*], Fangyan Dai[2], Valeria Berno[2], Adam T. Szafran[2], Kelly P. Smith[3], Tanmay Lele[4], Donald Ingber[4] and Michael A. Mancini[2,‡]

[1]Molecular Medicine, University of Texas Institutue of Biotechnology, San Antonio, TX, USA
[2]Molecular and Cellular Biology, Baylor College of Medicine, One Baylor Plaza, Houston, TX 77030, USA
[3]Department of Cell Biology, University of Massachussettes Medical School, Worcester, MA, USA
[4]Vascular Biology Program, Departments of Pathology and Surgery, Children's Hospital and Harvard Medical School, Boston, MA, USA
*These authors contributed equally to this work
‡Author for correspondence (e-mail: mancini@bcm.tmc.edu)

Accepted 5 July 2006
Journal of Cell Science 119, 000-000 Published by The Company of Biologists 2006
doi:10.1242/jcs.03161

Summary

We report a mammalian-based promoter chromosomal array system developed for single-cell studies of transcription-factor function. Designed after the prolactin promoter-enhancer, it allows for the direct visualization of estrogen receptor α (ERα) and/or Pit-1 interactions at a physiologically regulated transcription locus. ERα- and ligand-dependent cofactor recruitment, large-scale chromatin modifications and transcriptional activity identified a distinct fingerprint of responses for each condition. Ligand-dependent transcription (more than threefold activation compared with vehicle, or complete repression by mRNA fluorescent in situ hybridization) at the array correlated with its state of condensation, which was assayed using a novel high throughput microscopy approach. In support of the nuclear receptor hit-and-run model, photobleaching studies provided direct evidence of very transient ER-array interactions, and revealed ligand-dependent changes in k_{OFF}. ERα-truncation mutants indicated that helix-12 and interactions with co-regulators influenced both large-scale chromatin modeling and photobleaching recovery times. These data also showed that the ERα DNA-binding domain was insufficient for array targeting. Collectively, quantitative observations from this physiologically relevant biosensor suggest stochastic-based dynamics influence gene regulation at the promoter level.

Supplementary material available online at
http://jcs.biologists.org/cgi/content/full/119/??/????/DC1

Key words: Nuclear receptor, Prolactin, Chromatin, Co-regulator, Transcription, Photobleaching, Stochastics, Probabilistics

Introduction

Understanding transcription in the context of the nuclear environment has benefited from a combination of classic genetic systems and recent technological advances in molecular cell biology. A major goal is to document chromatin occupancy by transcription factors and other attendants at the molecular level, which can then be correlated with alterations in chromatin state and output from specific genes; however, cell-based inquiry of mammalian chromatin is limited. Nuclear receptors offer advantages in these pursuits because of their well-documented role in cellular responses to hormones.

Three experimental model systems in mammalian cells have been used to target transcription factors to integrated DNA. The spontaneous chromosomal integration of tandem mouse mammary tumor virus promoters in cell line 3617 (MMTV array) can be visualized using translational fusions of the green fluorescent protein (GFP) and the glucocorticoid receptor (GR) (McNally et al., 2000), the GR coactivator, GRIP-1 (Becker et al., 2002) and other transcription factors, including coactivators and a chromatin modifier (Muller et al., 2001). Chromosomally amplified *lac*-repressor-binding sites (*lac* arrays) have been used to visualize co-regulator interactions and chromatin changes in response to expression of a *lac* repressor, VP16 acidic activation domain and GFP chimera (Tumbar et al., 1999). An estrogen receptor α (ERα, herafter just called ER) chimera (GFP-lac-ER) was also used to document large-scale chromatin changes of the *lac* array in response to 17-β estradiol (E2) (Nye et al., 2002), and to record ligand-influenced, dynamic-recruitment of coactivators (Stenoien et al., 2001a). *lac* repeats linked to a repetitive Tet-responsive promoter were also recently used to observe chromatin changes in response to regulated activation of transcription (Janicki et al., 2004). In addition, live cell data using an HIV promoter array, and a synthetic NFκB binding site array, indicates rapid (seconds) oscillation of a gene regulator (NFκB) on a promoter (Bosisio et al., 2006). A general theme emerging from live single-cell studies of nuclear receptors and coactivators in individual mammalian cell nuclei is that their interactions (either at bulk chromatin or at specific DNA) are dynamic, with a half-time of residence in the order of seconds. The combined results of these model systems have greatly advanced our understanding of in vivo nuclear receptor (NR)-promoter, NR–co-regulator interactions and chromatin remodeling in general. However, each system individually lacks the ability to directly measure and correlate the multiple aspects of NR-mediated transcription, and has limited ability to assess antagonist-dependent transcriptional repression. The

development of a single system with these multiplex capabilities would facilitate a greater understanding of the molecular mechanisms involved in transcription in vivo.

Our goal for the work described here was to develop a system that allows us to analyze the live cell dynamics of ER, including promoter interactions and associated large-scale changes in chromatin. For this purpose, we used an integrated array of ER synergy elements located in the enhancer of the prolactin gene, which also contains a binding site for the POU-class activator Pit-1. In addition to being induced in vivo by estrogen (Carrillo et al., 1987), the prolactin gene is also repressed by antiestrogens (Lieberman et al., 1983). Additionally, prolactin chromatin structure was differentially altered by agonists and antagonists (Cullen et al., 1993; Seyfred and Gorski, 1990). Our results indicate the establishment of a single-cell model to visualize quantitatively the hormonal regulation of ER action and provide evidence in support of the hypothesis that stochastic ER-promoter interactions are crucial for transcriptional regulation.

Results

Large-scale ligand-mediated alterations in chromatin

Fig. 1 shows the DNA sequence of the prolactin promoter-enhancer region, and the Pit-1–ER synergy element that was multimerized in the construction of the plasmids used to establish our stable array-bearing reporter lines. To study large-scale chromatin changes, we treated GFP-ER-expressing PRL-HeLa cells with ligands or vehicle before imaging. We examined only cells with the lowest levels of fluorescence (typically the bottom 10% population, supplementary material Fig. S1C) to avoid overexpression artifacts. In this experiment, we quantitatively compared GFP-ER expression levels in PRL-HeLa cells with endogenous ER levels in MCF7 cells. The results indicated only a slightly greater level (<1.5-fold) of ER expression in PRL-HeLa cells relative to MCF7. In the experiments reported here, we ignored all transfected cells with levels of GFP-ER expression higher than that discussed above.

PRL arrays responded appropriately to antagonists by tight condensation (Fig. 2C,D), and to E2 by decondensation (Fig. 2B). E2-based decondensation contrasts with earlier results of multimerized *lac*-operator DNA using a *lac*-repressor–ER fusion (Nye et al., 2002). Most striking was the degree to which arrays condensed upon treatments with either the antiestrogens 4-hyrdroxytamoxifen (4HT; Fig. 2C) or ICI 182780 (ICI; Fig. 2D). These data revealed a remarkable plasticity in large-scale chromatin structure at the array, which appears similar to a smaller scale version of chromosome puffs. For an unbiased quantification of these responses, a high-throughput microscopy (HTM) approach was developed and applied to PRL-HeLa cells transiently expressing GFP-ER and treated with vehicle, E2 or 4HT (see Materials and Methods). Vehicle- and E2-treated cells had substantially larger size foci of fluorescence compared with 4HT and ICI, and E2 increased array size compared with vehicle (Fig. 2D). Time-lapse imaging demonstrated ligand-induced changes in array structure and illustrated real-time (minutes) decondensation (Fig. 3A) or condensation (Fig. 3B) upon exposure to agonist or antagonist, respectively.

Single-cell analyses of transcription by fluorescent in situ hybridization

For biological relevance, it was important to confirm transcriptional responses of the integrated PRL-based array to those previously documented for various ligand treatments in other systems. For this purpose, fluorescent in situ hybridization (FISH) was used to assay steady-state accumulation of reporter mRNA in response to ER expression and ligand (Fig. 4). Compared with non-transfected controls, there is a statistically significant higher level of array-associated reporter FISH signal in cells expressing wild-type ER in the absence of ligand. As expected from animal studies of pituitary responses to E2, the FISH signal localized at the PRL array increased at least 3.5-fold compared with vehicle controls within 30 minutes of exposure to E2. Interestingly, after 2 hours of ligand treatment, the level of induction was

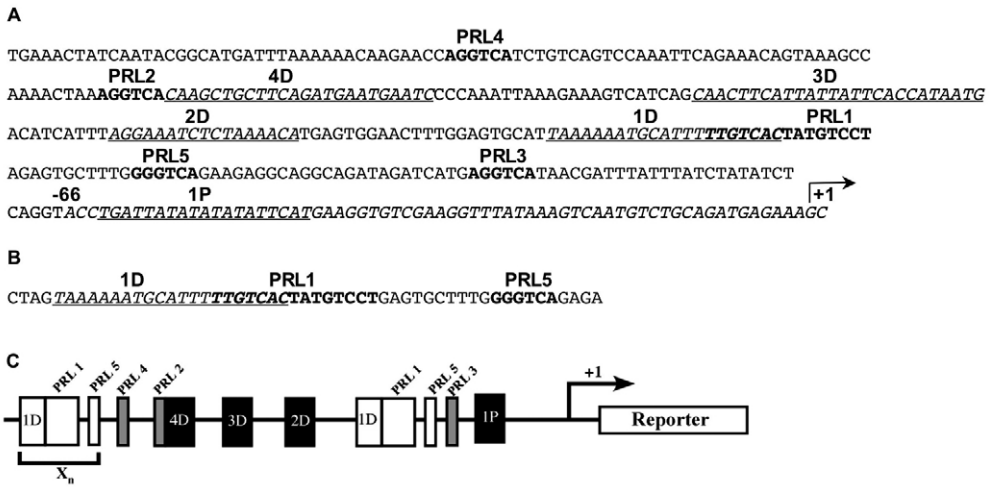

Fig. 1. PRL-based array construction and testing. (A) Sequence of the prolactin promoter (+1 to –66) with one high-affinity Pit-1-binding site (1P, italics and underlined) and enhancer (–1807 to –1498) that contains four Pit-1-binding sites (1D-4D, italics and underlined), and five EREs (PRL1-5, Bold text). (B) Sequence of the synergy element containing the Pit-1 1D site and two EREs (PRL1 and 5). (C) Schema showing the essential elements of the reporter constructions. Transcription start site, proximal promoter and enhancer sequence are shown in A. X_n indicates multimerized synergy elements denoting variable numbers of repeats (8, 13, 26, 52, 104).

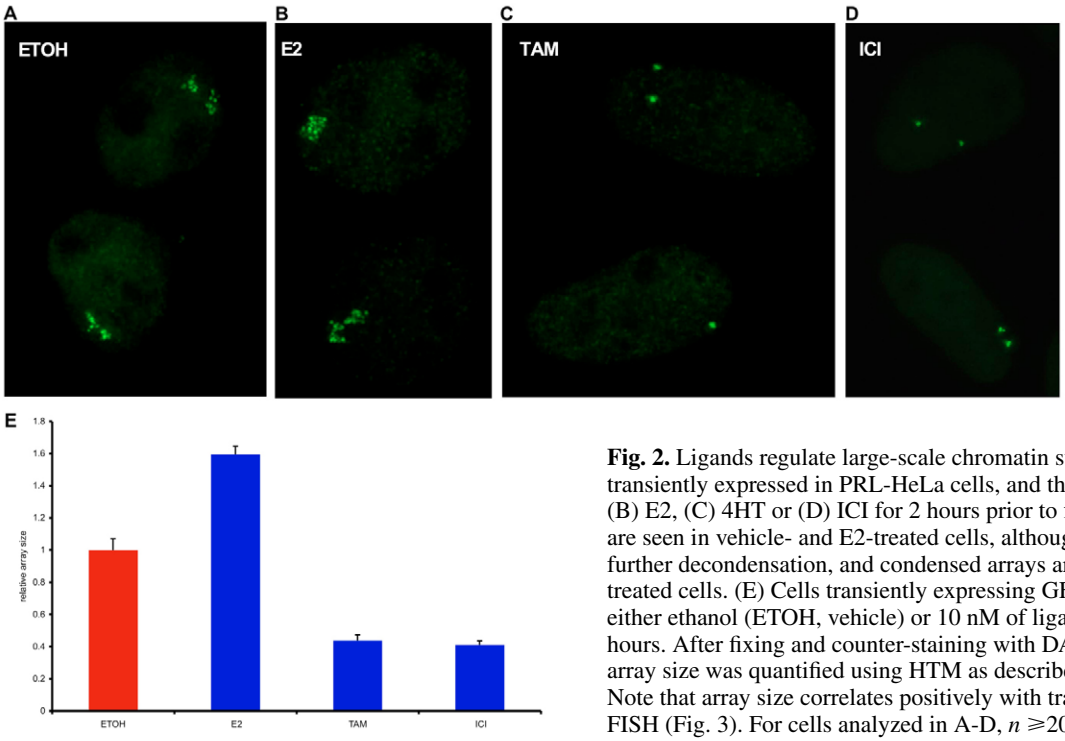

Fig. 2. Ligands regulate large-scale chromatin structure. (A-D) GFP-ER was transiently expressed in PRL-HeLa cells, and then treated with (A) ethanol, (B) E2, (C) 4HT or (D) ICI for 2 hours prior to fixation. Decondensed arrays are seen in vehicle- and E2-treated cells, although E2 treatment results in further decondensation, and condensed arrays are seen in 4HT- and ICI-treated cells. (E) Cells transiently expressing GFP-ER were treated with either ethanol (ETOH, vehicle) or 10 nM of ligand (E2, 4HT, ICI) for 2 hours. After fixing and counter-staining with DAPI, cells were imaged and array size was quantified using HTM as described in Materials and Methods. Note that array size correlates positively with transcription signal obtained by FISH (Fig. 3). For cells analyzed in A-D, $n \geqslant 200$; for HTM, n=500.

substantially higher than vehicle (more than twofold), but was reproducibly lower than the 30-minute treatment. Further demonstrating the hormonal responsiveness of the array, and correlating tightly to array size, 4HT and ICI completely repressed basal array FISH signal in the presence of ER. In the absence of ER, these antagonists had no effect on the array in terms of its size or constitutive levels of transcription (data not shown). The multiple, small FISH-signal foci in the 4HT-treated cells (arrows, Fig. 4B) are separate from the PRL array and were observed sporadically in cells under all treatment conditions. Importantly, the combination of array size and FISH data provided an early demonstration that ligand treatments lead to expected responses to agonist (decondensation of the array and increase in FISH signal) and antagonists (significant condensation of the array and undetectable FISH signal) (Figs 2 and 4, respectively). These data, which mimic the endocrinological response (e.g. agonist induction and antagonist repression) to hormones in the pituitary, provided confidence for the use of the multicopy, modified PRL promoter-enhancer in additional studies of the nuclear dynamics of ER and association of transcription co-regulators with the array.

Co-regulator and RNA polymerase II targeting, and modified histones

To further assess the biological significance of transcriptional responses of the PRL array, we performed immunolocalization studies using a series of antibodies directed against endogenous transcription factors, cofactors and modified histones. The p160 class coactivators (SRC-1 and SRC-3) accumulated over the array (versus nucleoplasmic levels) when GFP-ER without ligand or bound to E2 associated with the array (Fig. 5). In the absence of GFP-ER, neither of the p160 coactivators accumulated over the array (Fig. 5). As expected from previous lacER-p160 studies (Stenoien et al., 2001a), antagonist treatment resulted in a loss in accumulation of p160 coactivators at GFP-ER-occupied PRL arrays; interestingly, relative to SRC-3, reduction of SRC-1 was not always as robust with 4HT or ICI (Table 1, supplementary material Fig. S3). Similar assays were performed for the chromatin remodeling protein BRG1, which interacts with ER and is required by glucocorticoid receptor for chromatin remodeling (McKenna et al., 1999). BRG1 accumulated over the array with GFP-ER in vehicle-treated and E2-treated cells, but was not detected at arrays in antagonist-treated cells (Fig. 6, Table 1). Thus, each of these factors previously identified to be important for transcription activation appeared to have a unique signature of receptor- and ligand-dependent accumulation over the array.

In line with constitutive activity from the integrated transcription unit, the transcription elongation factors cyclin T1, CDK9 (Table 1; supplementary material Figs S4, 5) and the large subunit of RNA polymerase II (RNAPII) (Fig. 7) each showed array-associated targeting in non-transfected PRL-

Table 1. Summary of ER, coregulator and RNAPII accumulation at the array

	Non-transfected	Vehicle	E2	4HT	ICI	Antibody
GFP-ER	–	+	+	±	±	SRC-1
	–	±	+	–	–	SRC-3
	–	+	+	–	–	BRG1
	+	+	+	–	–	Cyclin T1
	+	+	+	–	–	CDK9
	+	+	+	–	±	RNAPII

PRL-HeLa cells were mock-transfected or transfected transiently with GFP-ER expression plasmids. Subsequently, the cells were treated with vehicle or the indicated ligands (10 mM, 2 hours). +, colocalization with GFP-ER fluorescence; –, no colocalization detected; ±, partial colocalization.

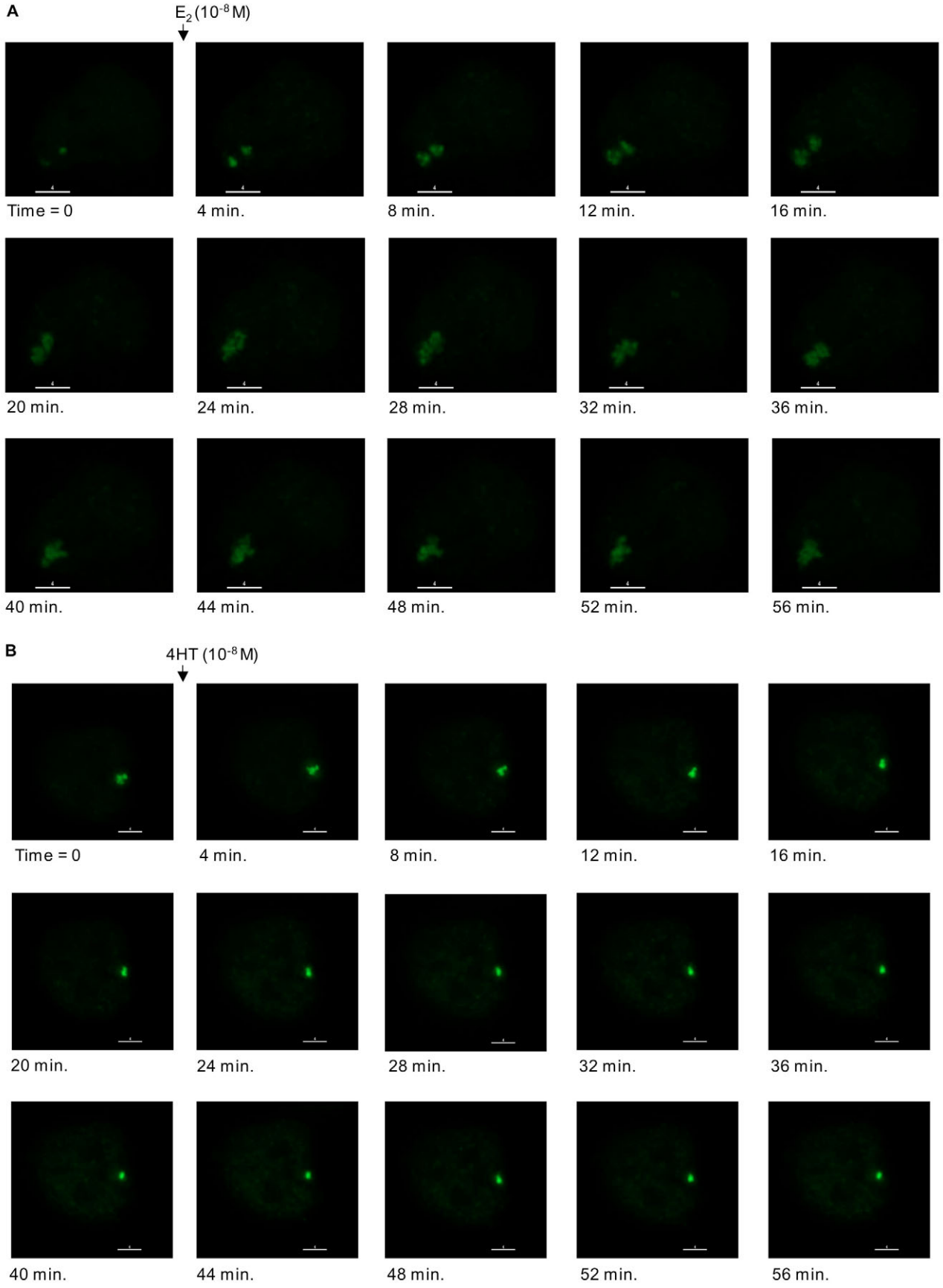

Fig. 3. See next page for legend.

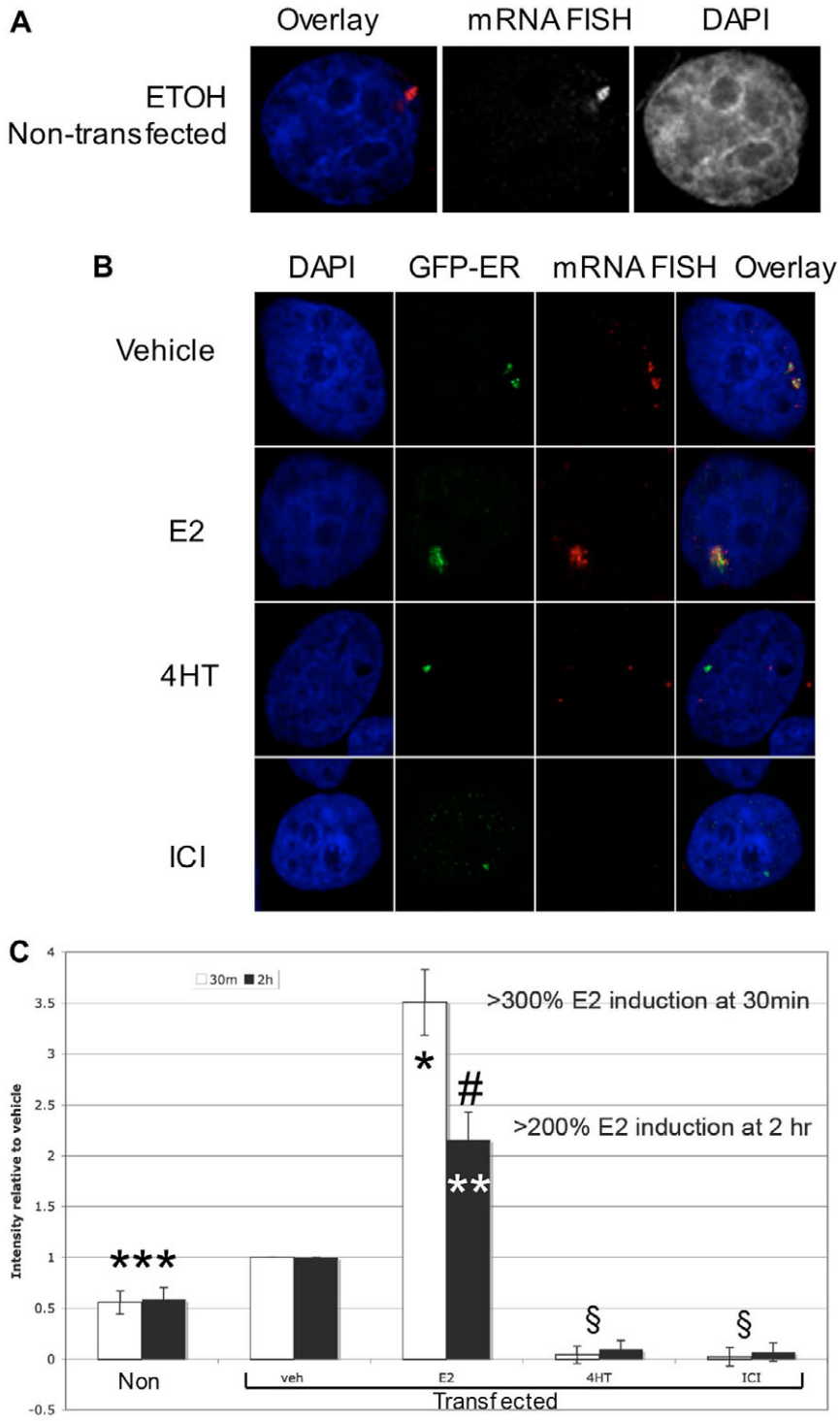

Fig. 3. Real-time visualization of alterations in chromatin structure of the GFP-ER-targeted PRL array in response to E2 or 4HT. Time-lapse images were obtained by deconvolution microscopy using live cells transiently expressing GFP-ER. Ligand addition is indicated after t=0, and frames are labeled with time points after t=0. The images were deconvolved and those shown are projected image stacks. (A) Typical data from PRL-HeLa cells treated with E2. (B) Data from PRL-HeLa cells treated with 4HT. n=10 for cells analyzed. The size bar indicates length in microns.

Fig. 4. Single-cell analyses of the transcriptional response of the PRL array to ligands. (A,B) Cells were (A) mock-transfected or (B) transiently transfected with GFP-ER expression plasmid. Cells in B were treated with vehicle or the indicated ligands (10 nM) for 2.5 hours, processed for FISH and imaged as described in Materials and Methods. GFP-ER signal is shown in green, mRNA FISH signal is shown in red. Overlay includes DAPI-stained nuclei (blue). Two of the small multiple foci of FISH signal in this 4HT-treated cell are marked with white arrows. (C) The FISH signals at the array were quantified as described in Materials and Methods and shown as bar graphs. Treatments (30 minutes, white bars and 2 hours, black bars) are indicated below the graphs; 'Non' and 'Transfected' indicate mock- and transfected cells, respectively. FISH signals at the array were quantified in 20 cells for each treatment as relative intensity of the cells treated with vehicle and are shown as bar graphs. While there is constitutive level of FISH signal (A), it increases significantly in cells with arrays demarcated with GFP-ER. *P=0.007, E2-treated GFP-ER-expressing cells at 30 minutes compared with vehicle controls. **P<0.001, E2-treated GRP-ER-expressing cells at 2 hours compared with vehicle controls. ***P=0.0016, non-transfected cells compared with GFP-ER-expressing cells. $^{\#}P$=0.0378, 30 minutes compared with cells treated 2 hours with E2. $^{\S}P$<0.001, antagonist-treated GFP-ER-expressing cells versus vehicle controls.

HeLa cells. By contrast, cells expressing GFP-ER and treated or not with E2 showed an increased accumulation of these factors over the array. Consistent with FISH results described above, exposure to 4HT or ICI eliminated the accumulation of cyclin T1 and CDK9 from GFP-ER targeted arrays. Similarly, 4HT resulted in loss of RNAPII accumulation at GFP-ER-targeted arrays and ICI treatment was not as effective in abolishing RNAPII array accumulation (Fig. 7).

We also characterized ligand-dependent histone modifications at the PRL array by immunofluorescence. Histone acetylation is associated with estrogen receptor activation (Kim et al., 2001), and histone methylation is associated with both transcriptional activation and repression (reviewed by Kouzarides, 2002). In cells not expressing exogenous estrogen receptor, acetylation of histone H3 at the array was observed (Fig. 8). This is indicative of a low level of constitutive transcription at the array (confirmed by colocalization with dsRed2 RNA FISH, data not shown). Surprisingly, GFP-ER-targeted arrays with or without ligands did not dramatically alter the levels of acetylated histone H3 array accumulation, even when highly condensed by 4HT or ICI (Fig. 8). Similar results were obtained for transcription-associated dimethyl-lysine of histone H3 (Fig. 9). Repression-

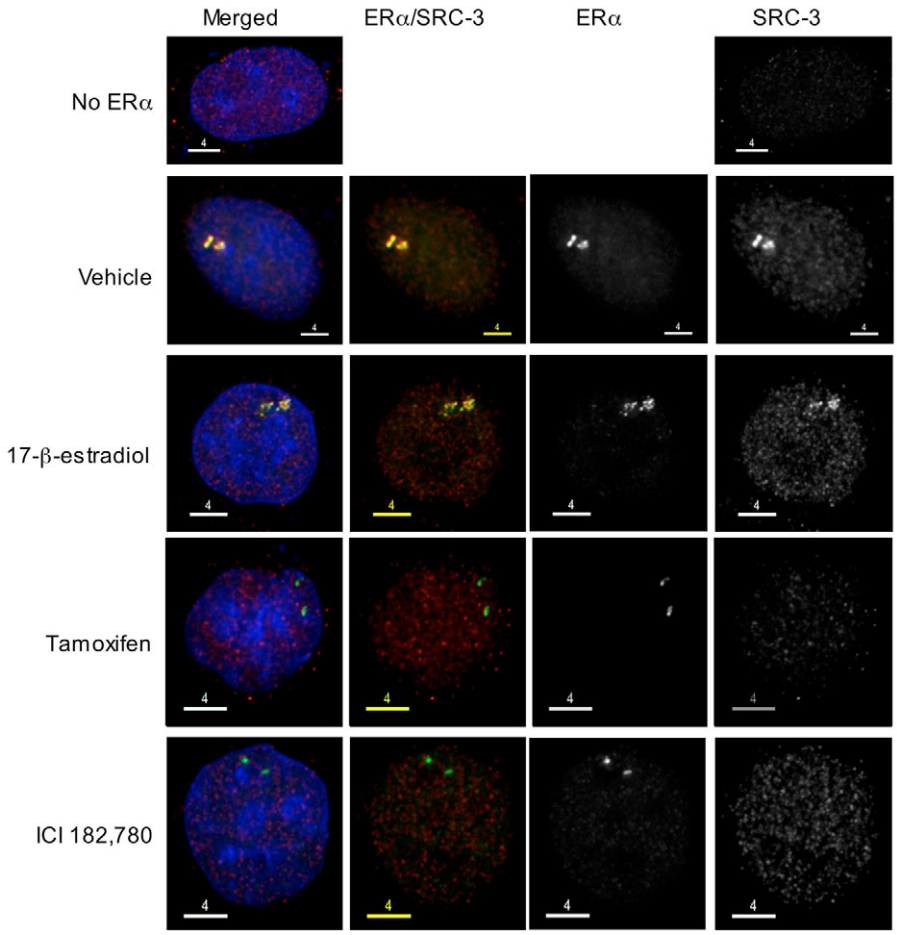

Fig. 5. Colocalization of SRC-3 coactivator and GFP-ER at the PRL array. PRL-HeLa cells transiently expressing GFP-ER were treated with vehicle or the ligands indicated (10 nM, 2 hours). Afterwards the cells were immunostained for SRC-3. The fluorescent signal origin is labeled above the panels and merged images include DAPI-stained nuclei. $n \geqslant 200$ for cells analyzed. The size bar indicates length in microns.

associated dimethyl-lysine 9 of H3 was not observed on condensed arrays at levels above those in the nucleoplasm, neither was acetylated histone H4 observed at the array under any ligand condition (data not shown).

In sum, these data on association of cofactors under varying conditions are consistent with the transcription responses observed by reporter FISH, and suggests that the integrated multicopy promoter-enhancer array responded to ER and its ligands in a biologically appropriate manner, albeit with characteristics specific for the prolactin promoter-enhancer.

Ligands affect ER mobility at prolactin array

To better confine real-time measurement of ER dynamics to a smaller nuclear volume containing a specific transcription locus, versus bulk nucleoplasm (Reid et al., 2003; Stenoien et al., 2001b), we examined live cell dynamics of GFP-ER at the PRL promoter array by fluorescence recovery after photobleaching (FRAP) methods.

Initially, we transiently transfected GFP-ER and performed a spot-FRAP analysis in both the nucleoplasm and at the array. As in our earlier studies, with minimal media (charcoal-stripped and dialyzed serum-containing), photobleaching the nucleoplasm demonstrated that ER mobility was extremely fast, with a half-maximal recovery ($t_{1/2}$) of less than 1 second. The addition of E2 or 4HT resulted in significant reduction of ER mobility within the nucleoplasm (E2, 5 seconds; 4HT, 4 seconds) and, as expected, ICI immobilized ER (Table 3, data not shown). With improved normalization and analytical methods (see Materials and Methods), and in refinement of our previous work, we report here that 4HT led to a small but significant increase in mobility throughout the nucleus compared with E2.

FRAP was also used to specifically measure mobility over the PRL array (Fig. 10A,D; Table 2). GFP-ER recovery was markedly slower than that of nucleoplasmic receptor or Pit-1 (Fig. 10C). In the absence of ligand, $t_{1/2}$ of GFP-ER was 12.19±1.92 seconds, n=30, which, interestingly, was not significantly different from that observed in the presence of E2 (11.64±3.41 seconds, n=30). 4HT treatments significantly increased mobility of array-associated GFP-ER (10.56±1.70 seconds, n=30), in concert with dramatic alterations in array size, the composition of recruited proteins and reductions of reporter mRNA shown above. As with nucleoplasmic receptors, ICI immobilized array-associated GFP-ER (Fig. 10A,D; Table 2).

Owing to concerns that the recovery dynamics observed at the de-condensed arrays could have been affected by the larger amount of bulk nucleoplasm interspersed with array chromatin, we reduced bleach regions to an area the size of the 4HT-induced condensed arrays. Because this meant that partial regions of larger arrays were photobleached, we refer to these as intra-array FRAP ($FRAP_{intra\text{-}array}$). As shown in Table 2, $FRAP_{intra\text{-}array}$ data qualitatively agreed with the FRAP results above (absolute differences were due to different analysis method, see Methods and Materials), and demonstrated that differences in ER mobility were not the trivial result of differently sized arrays or bleach regions, or to the contribution of bulk nucleoplasmic dynamics in general.

FRAP and $FRAP_{intra\text{-}array}$ data provided recovery rates that represented both on- and off-rates of the photobleached proteins. To more directly assess GFP-ER loss from the array, we used inverse FRAP (iFRAP) (Becker et al., 2002; Dundr et al., 2002). In iFRAP, the entire nucleus, excluding the array, is bleached (Fig. 10B), and loss of fluorescence is directly related to the dissociation kinetics of GFP-ER from array chromatin. In absence of ligand, half-maximal loss ($t_{1/2\text{-}loss}$) of GFP-ER fluorescence was 4.55±2.54 seconds, n=30) (Table 2). In contrast to FRAP or $FRAP_{intra\text{-}array}$, addition of E2 resulted in a marked and significant (>50%, P<0.001) increase in $t_{1/2\text{-}loss}$

(6.49±1.79 seconds, n=30) (Fig. 10E, Table 2). iFRAP after treatment with 4HT, however, resulted in faster $t_{1/2\text{-loss}}$ than after treatment with E2 (4.11±0.85 seconds, n=30) (Fig, 10E, Table 2). Consistent with FRAP analyses, iFRAP also indicated that ICI immobilized GFP-ER in association with the array (data not shown).

In vivo mapping of ER domains required for array targeting

We next used PRL-HeLa cells to ask whether well-defined domains of ER contribute to the dynamics of GFP-ER interactions with array chromatin. ER domains associated with subnuclear localization, solubility and mobility have been previously reported (Stenoien et al., 2000; Stenoien et al., 2001a), with helix-12 of the ligand-binding domain (LBD) being implicated as a key intranuclear regulatory interface in living cells. To test this model with a biologically relevant, visible chromatin locus, we transiently introduced a GFP-ER-deletion series, including: (1) GFP-ER_{282} (AF1 with the DNA-binding domain, DBD), (2) GFP-ER_{534} (AF1, DBD and LBD up to, but excluding, helix-12) and, (3) GFP-ER_{554} (AF1, DBD and LBD including helix-12), Fig. 11A. In vitro and in vivo assays showed that GFP-ER_{554} retains agonist-inducible transcription function on an estrogen response element (ERE)-dependent reporter (Pakdel et al., 1993), whereas GFP-ER_{282} and GFP-ER_{534} are transcriptionally inactive (Tzukerman et al., 1994). In vitro, all deletion mutants bind DNA in an electrophoretic mobility shift assay (EMSA), and ER_{534} and ER_{554} bind ligand, whereas ER_{282} does not.

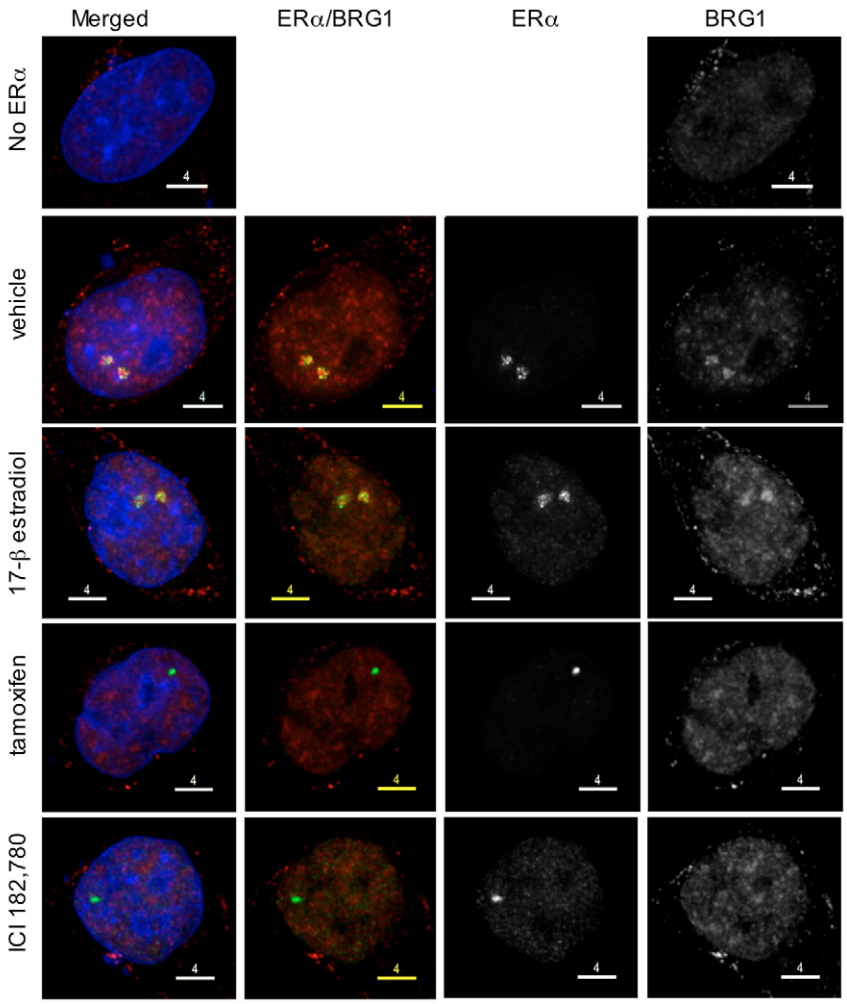

Fig. 6. Colocalization of BRG1 chromatin modifier and GFP-ER at the PRL array. Representative PRL-HeLa cell images transiently expressing GFP-ER and immunostained for BRG1. Cells were treated and images were obtained and presented as in Fig. 4. $n \geqslant 200$ for cells analyzed. The size bar indicates length in microns.

In stark contrast to its ability to bind DNA in EMSA, GFP-ER_{282} failed to demonstrate any detectable targeting to the PRL array (Fig. 11B). In the presence of E2, but not vehicle, GFP-ER_{534} associated with the PRL array, further supporting the ligand-binding potential of the truncated LBD. However, PRL arrays demarcated with GFP-ER_{534} remained condensed (Table 3) and showed no detectable recruitment of RNAPII (data not shown). Conversely, GFP-ER_{554} targeted the array indistinguishably from wild-type ER (Fig. 11B) and responded to 4HT and ICI, as evidenced by array condensation (Table 3).

Estrogen receptor domains contribute to its nucleoplasmic and PRL array dynamics

Our panel of mutated receptors was next analyzed for mobility in the nucleoplasm and at the PRL array. As we have shown previously (Stenoien et al., 2001b), GFP-ER_{282} was very mobile in the nucleoplasm and, as expected, unaffected by ligand (Fig. 11C, Table 5). Unliganded GFP-ER_{534} was also very mobile in the nucleoplasm and was significantly reduced by E2 (Fig. 11C, Table 4). GFP-ER_{554} demonstrated slower nucleoplasmic mobility relative to GFP-ER_{282} and GFP-ER_{534}, consistent with a role for helix-12, and also exhibited reduced mobility upon exposure to E2 (Fig. 10C, Table 4). At the PRL array, GFP-ER_{554} demonstrated significantly faster recovery compared with GFP-ER in cells treated with vehicle (Fig. 11C, Table 4), similar to its faster reorganization into nucleoplasmic hyperspeckles after addition of E2 (Stenoien et al., 2001a). In cells treated with E2, GFP-ER_{534} demonstrated the fastest recovery times at the array, followed by GFP-ER and GFP-ER_{554} (Fig. 11C, Table 4).

Discussion

We present here, for the first time, a direct and quantitative evaluation of spatiotemporal issues involved in transcription from a entirely mammalian promoter-enhancer array. The modified PRL promoter-enhancer array responds in a physiologically relevant manner to ER and ligands in terms of reporter-mRNA transcription. Its activity is linked to live cell dynamics of the receptor at the transcription locus and to readily measurable alterations in large-scale chromatin structure. Since ER is located predominantly in the nucleus,

our system affords a new level of interrogation of transcription factor interactions with an integrated locus, both in the context of agonist-induced transcription and antagonist-induced repression. Further, this approach demonstrates that a transcriptional biosensor can be constructed from mammalian promoter components and establishes the feasibility of creating similar test systems with other types of DNA-binding factors that mediate transactions with chromatin. In addition to being an integrated reporter of chromatin structure-function relationships, arrays are highly amenable to analytical tools, including HTM as performed for this report, and should be a harbinger for systems-biology-level-approaches to transcription.

As we (Stenoien et al., 2000; Stenoien et al., 2001a; Stenoien et al., 2001b) and others (Htun et al., 1999) have shown, ligand exposure within minutes affects intranuclear targeting and dynamics of ER, with maximal reorganization peaking at about 30 minutes. Here, we more directly observed hormonally regulated transcriptional events at the integrated array, including remarkable ligand-dependent size and/or density plasticity of array chromatin marked by GFP-ER, which are tightly correlated to the ligand-regulated activation or repression of the array (Figs 1, 2). We are examining the potential of using HTM in live cell experiments to capture unbiased quantitative data on a large number of cells to assess array-size dynamics under variable experimental conditions similar those in Fig. 2. We currently interpret changes in array size as a reflection of alterations in chromatin state (closing and opening) that correlate directly with ER-mediated differences in transcriptional output and colocalization of RNAPII and its cofactors. The rapid loss of most of these factors from the array in response to antagonists is mechanistically consistent with marked changes in array size and undetectable levels of dsRED2skl mRNA by FISH.

Our ligand-based activation and repression studies document an interesting pattern of array-associated coactivators, chromatin modification enzymes, transcription elongation factors and RNAPII. Accumulation over the PRL array by cyclin T1, CDK9 and RNAPII is specific for transcription, be it constitutive or agonist enhanced. One unexpected observation was the incomplete disassociation of RNAPII from the PRL array chromatin in cells treated with the pure antagonist ICI. The interaction is antagonist-specific, because 4HT treatment reduced RNAPII association to nucleoplasmic levels. As neither cyclin T1 nor CDK9 is detected at arrays in ICI-treated cells, our data suggest that RNAPII is not activated (pre-initiation complex), is in an abortive cycle or is perhaps trapped with immobilized GFP-ER. The apparent association of the p160 coactivators, SRC-1 and SRC-3 is also not as straightforward. In our immunoassays of GFP-ER-expressing cells, colocalization with the array by SRC-3 appears to be strictly receptor dependent, and is regulated by agonist (increased SRC-3) and antagonist (dissociated SRC-3). SRC-1 colocalization, however, appears to be receptor-dependent (with or without agonist), and at least partially resistant to antagonist dissociation. It will be important to extend these immunoassays with experiments using fluorescently tagged SRC coactivators in photobleaching and protein-protein (FRET) studies to establish interactions following transcriptional stimulation or repression.

Significant changes in array size and/or density do not accompany major changes in several histone modifications that we have assayed. Previous histone modification studies have shown changes in acetylation of histone H3 or H4 after targeting repetitive, heterochromatic *lac* operator arrays directly with *lac* repressor-activator fusions (e.g. lacVP16, lacer) (see Nye et al., 2002; Tumbar et al., 1999). Also, a combined *lac* operator and *tet* operator array system regulated by tetOn also demonstrated histone modifications in *cis* (Janicki et al., 2004; Tsukamoto et al., 2000). With our studies, however, despite significant differences in array size (Figs 1, 2), acetylation and dimethylation of lysine 4 of histone H3 is not dramatically altered in immunofluorescence assays. Moreover, acetylation of histone H4 over the PRL array was never observed above nucleoplasmic levels. Finally, we examined the

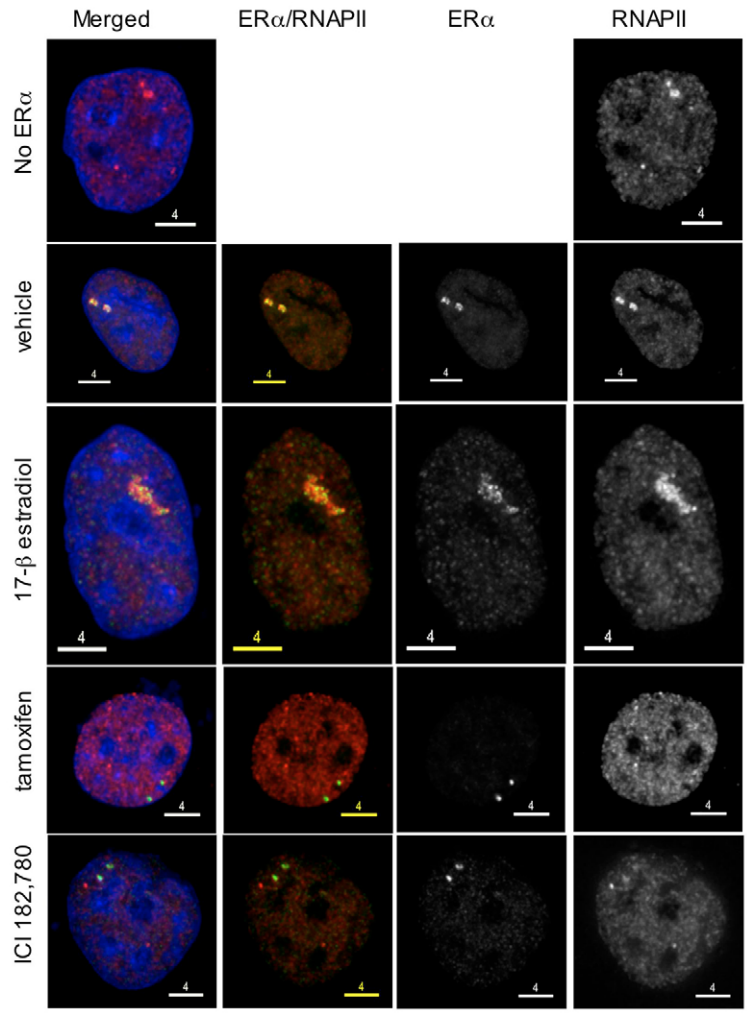

Fig. 7. Colocalization of RNAPII large subunit and GFP-ER at the PRL array. Representative PRL-HeLa cell images transiently expressing GFP-ER and immunostained for RNAPII. Cells were treated and images were obtained and presented as in Fig. 4. $n \geqslant 200$ for cells analyzed. The size bar indicates length in microns.

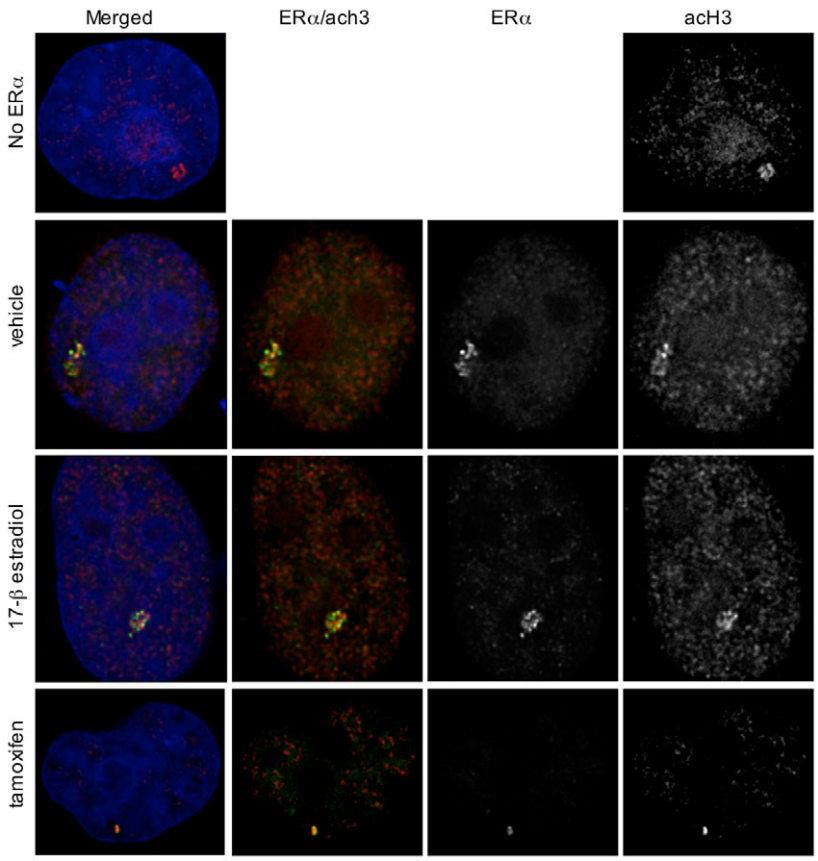

Fig. 8. Colocalization of acetylated histone H3 (acH3) and GFP-ER at the PRL array. Representative PRL-HeLa cell images transiently expressing GFP-ER and immunostained for acH3. Cells were treated and images were obtained and presented as in Fig. 4. For cells analyzed, $n \geqslant 200$.

repression-associated methylated histone H3 (at lysine 9) and also did not see significant array signal above nucleoplasmic levels when the locus was repressed and highly condensed by 4HT or ICI (data not shown). One possibility is that minor changes in histone modification are not detectable by our assay, although such changes have been documented using biochemical approaches. Another possibility is that chromatin on the scale observed here may not be primarily mediated by changes in the acetylation and/or methylation of histones, but rather other modifications such as ADP-ribosylation (Tulin and Spradling, 2003), for which we are in the process of assaying. Also, the lack of changes may represent a form of memory in the histone code. Indeed, we are actively investigating the possibility of ligand-dependent delays in large-scale chromatin modification in hormone-switching experiments. It is also possible that, direct single-cell analyses give different results than cell-population-based biochemical (ChIP) studies that average results from millions of cells. In this vein, the ER molecular dynamics reported here, as with GR (McNally et al., 2000), differ substantially (range of seconds) from ChIP results (tens of minutes) (Metivier et al., 2003; Reid et al., 2003; Shang et al., 2000). Finally, it is possible that analyses beyond 2-hour time points can more readily show changes in histone modifications. Development of quantitative imaging approaches to better assess histone modifications at the PRL-array are required to help address this issue. Further, analyses of similarly created, hormonally responsive transcription biosensor lines containing other nuclear receptor-targeted arrays will also assist in better understanding these issues.

Accumulating evidence supports a non-ligand-dependent transcription function for ER (reviewed in Coleman and Smith, 2001). Thus, whereas it was not surprising to

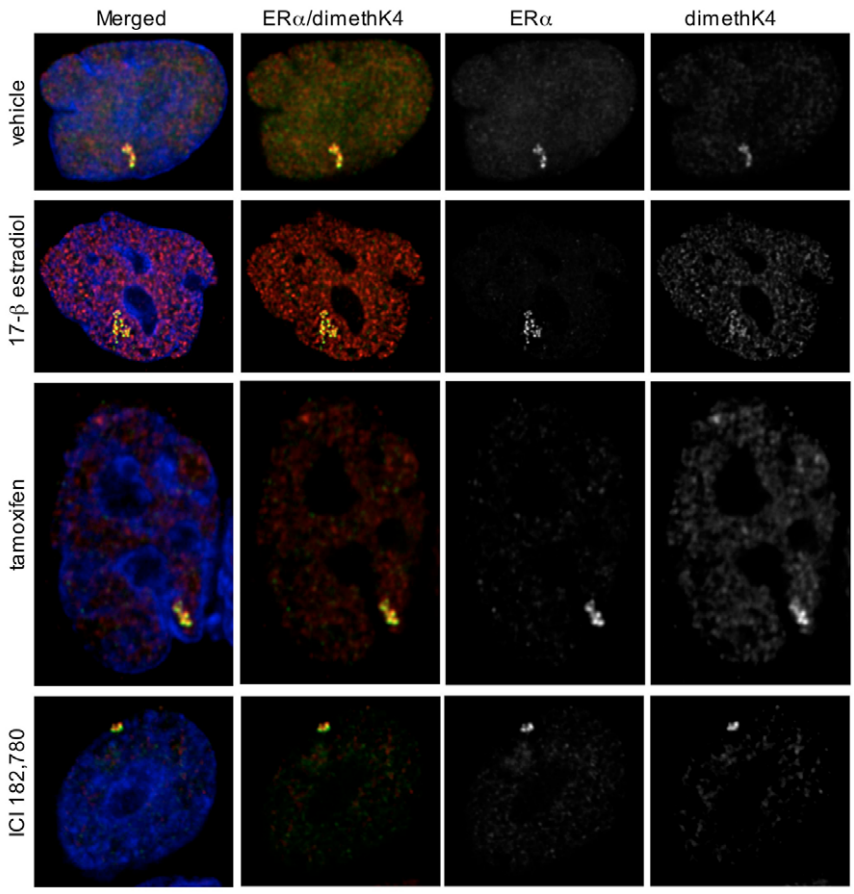

Fig. 9. Colocalization of histone dimethylated at lysine residue (dimethK4) and GFP-ER at the PRL array. Representative PRL-HeLa cell images transiently expressing GFP-ER and immunostained for dimethK4. Cells were treated and images were obtained and presented as in Fig. 4. $n \geqslant 200$ for cells analyzed.

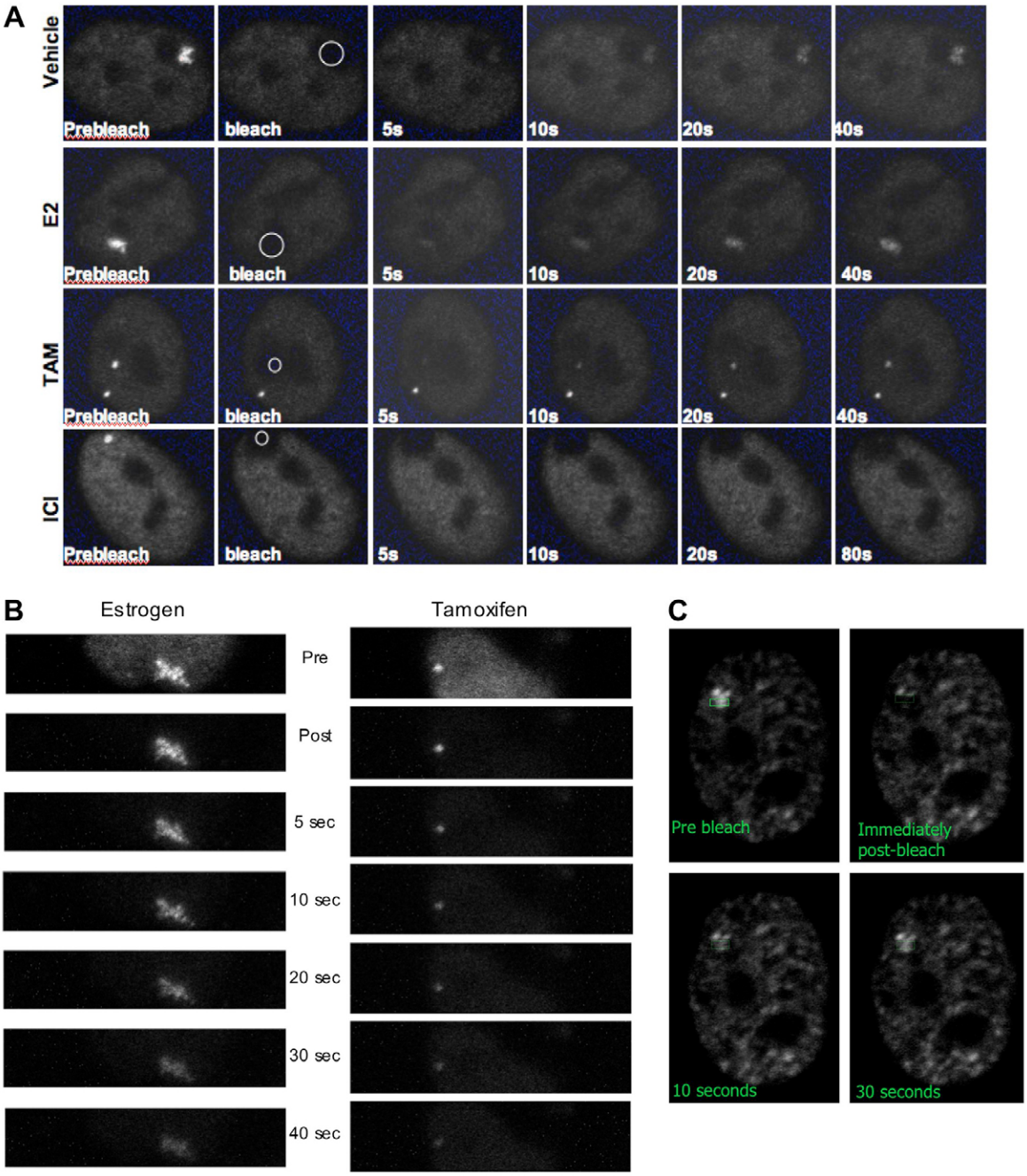

Fig. 10. ER and Pit-1 mobility over PRL array. (A) Representative time-lapse images of photobleaching and recovery of GFP-ER-targeted arrays (FRAP). FRAP was used to examine GFP-ER at the PRL array and in the surrounding nucleoplasm (images not shown). PRL-HeLa cells transiently expressing GFP-ER were treated with vehicle or ligands at 10 nM for 2 hours. Pre-bleach and bleach refer to cells before and after photobleaching. Time in seconds after bleaching is indicated. (B) Representative time-lapse images of nuclear photobleaching and loss of GFP-ER from targeted arrays (inverseFRAP). In these experiments, PRL-HeLa cells transiently expressing GFP-ER were treated with E2 (Estrogen) or 4HT (Tamoxifen). Pre and Post refer to images acquired prior to and immediately post photobleaching; time after post-bleach is indicated in seconds. (C) PRL-HeLa cells transiently expressing GFP-Pit-1 were analyzed by FRAP as described in A. (D) FRAP recovery curves are shown for nucleoplasm (left) and PRL array (right) in cells transiently expressing GFP-ER and treated with vehicle (No ligand), E2, 4HT (Tam) and ICI. The initial fluorescence immediately before the bleach was normalized to 1 and the curve starts from the time point immediately after the bleach. Note that non-ligand-dependent interactions greatly slowed the recovery of receptor over the PRL array compared with nucleoplasm, but E2 did not additionally decrease recovery times of GFP-ER at the array. 4HT lead to faster recovery both on and off the array. ICI, as expected, immobilized GFP-ER in the nucleus. (E) iFRAP loss curves were obtained in a similar manner, except that prebleach values were retained. PRL-HeLa cells transiently expressing GFP-ER were treated with vehicle, E2 or 4HT (10 nM) prior to photobleaching. The fluorescence at the PRL array was averaged over a 60-second time frame. The initial fluorescence immediately after photobleaching was normalized to 1 and relative fluorescence before bleaching was set to zero. k_{Off} was slower with E2 than no ligand or 4HT. n=30 for FRAP analysis under each condition.

frequently observe non-liganded ER interacting with the arrays, it was interesting that unliganded receptor appeared to mediate significantly higher level of colocalizing reporter mRNA. Notably, there is a significant change in mobility of unliganded GFP-ER in the nucleoplasm versus over the PRL array (<1 second versus ~12 seconds, respectively). Ligand-dependent activation data are consistent with an increase in the number of cells with GFP-ER targeted arrays after treatment with E2 (from ~75% to >99%, supplementary material Fig. S2C).

Together, both FRAP and iFRAP data show that the fluorescently tagged nuclear receptor ER and the POU-class activator Pit-1 exhibit short resident times on a promoter-enhancer-based array, similar to the GFP-GR results reported using both the MMTV (McNally et al., 2000) and HIV array (Bosisio et al., 2006). An advantage in this system is the opportunity to document the molecular dynamics under conditions of both antagonists and agonist. In the case of ER and the PRL array, it was striking to find that ligand significantly influenced its time of residence. Whereas FRAP data from our lab (Stenoien et al., 2001b) and others (Reid et al., 2003) have shown that intra-nuclear mobility of ER is regulated by ligand, proteasome function or ATP, these data reflect the sum of multiple interactions in the nuclear volume that contains (spatially) few ER target genes. Nevertheless, we were surprised that E2 did not significantly change the 'dwell time' over transcriptionally active array by standard FRAP. This result might represent a canceling out of putative, E2-

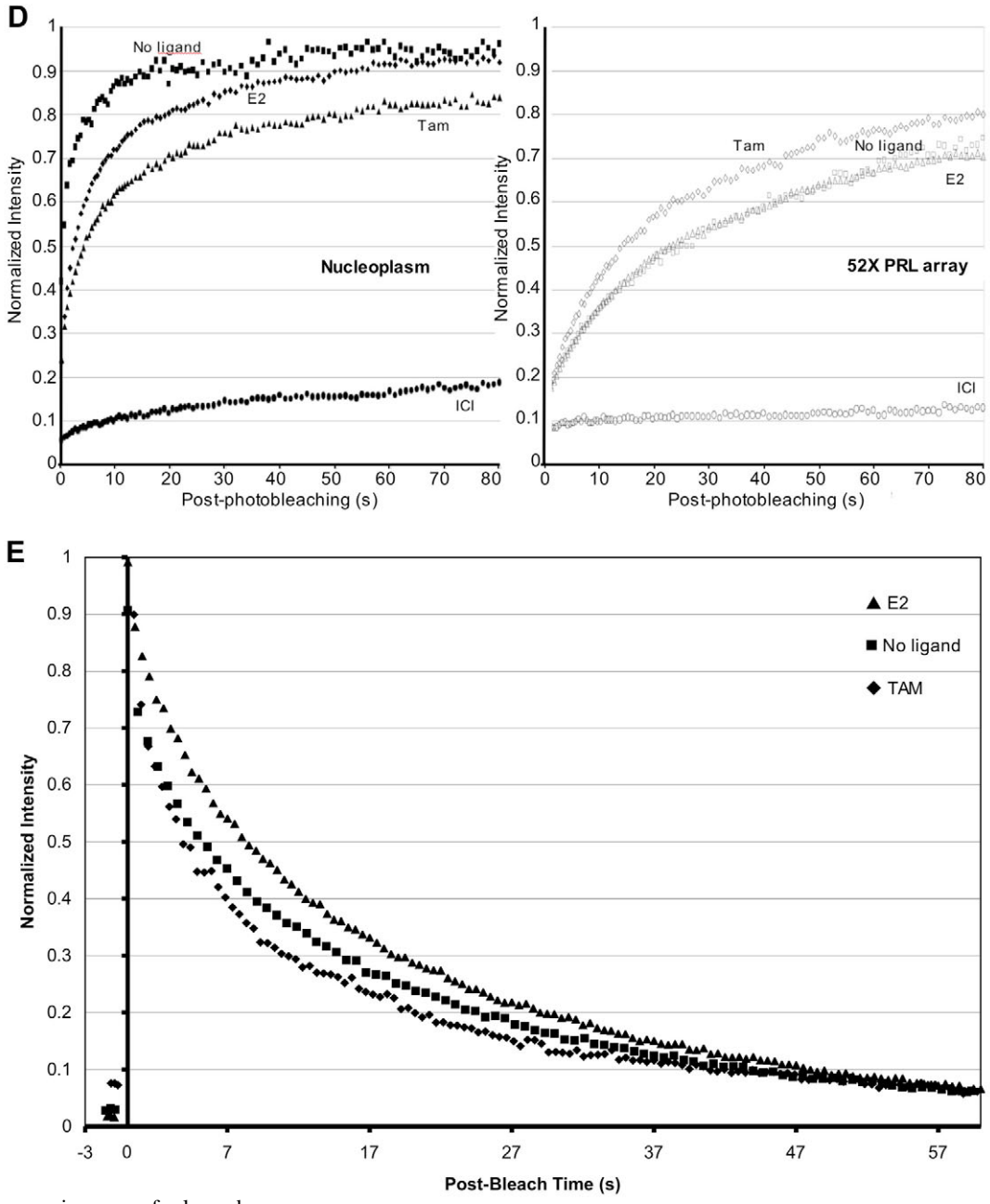

Fig. 10D,E. See previous page for legend.

Table 2. Summary of photobleaching results of GFP-ER

	Mean $t_{1/2}$	s.d.	s.e.m.	*n*	R^2
FRAP, nucleoplasm*					
No ligand	0.94	0.08	0.02	18	0.890
E2	5.28	0.85	0.32	7	0.991
4HT	3.70	1.22	0.3	17	0.983
FRAP, array**					
No ligand	12.19	1.92	0.4	23	0.936
E2	11.64	1.63	0.33	25	0.951
4HT	9.65	2.17	0.49	20	0.968
FRAP, intra-array**					
No ligand	5.77	2.26	0.44	27	0.789
E2	3.46	0.97	0.21	22	0.775
4HT	2.24	0.63	0.15	18	0.780
iFRAP, array***					
No ligand	4.55	2.54	0.397	41	0.992
E2	6.49	1.79	0.246	53	0.997
4HT	4.11	0.85	0.111	58	0.964

PRL-HeLa cells were transfected transiently with GFP-ER expression plasmids. Subsequently, the cells were treated with vehicle or the indicated ligands (10 nM, 2 hours). The mean half maximal ($t_{1/2}$) FRAP recovery or iFRAP loss are indicated. Nucleoplasmic- and array-associated FRAP data are indicated. Intra-array FRAP indicates recovery of defined regions of the focus of fluorescence, which was done in an attempt to control for size when comparing FRAP data obtained from condensed arrays in 4HT-treated cells.

*P<0.001, significant difference between all treatment conditions; **P<0.05, significant difference between E2 and 4HT, and between no ligand and 4HT; ***P<0.001, significant difference between E2 and no ligand, and between E2 and 4HT.

mediated changes of (1) on- and off-rates of DNA-binding, (2) ER dimerization, (3) protein recruitment or, (4) proteasome-mediated turnover. Although we addressed potential trivial caveats of array size influencing mobility values using $FRAP_{intra\text{-}array}$, we feel it is clearer to interpret ligand effects using the more focused k_{OFF} data obtained from iFRAP. Our results from this approach show that the array dwell time is significantly increased after E2 treatment compared with vehicle or 4HT. This would be consistent with E2 promoting productive (additional) interactions at target promoters rather than increasing promoter binding. Differential GFP-ER array-dwell-time might represent assembly and disassembly of the focal and, probably very transient, nuclear receptor complexes, representing important mechanistic steps in regulating transcription and associated large-scale chromatin alterations. We interpret these live cell findings of activation- or repression-associated ER to be an important extension of the previously supported hit-and-run model of transcription activation by ligand-activated GR at the MMTV array (McNally et al., 2000). We also noticed significant agreement in the beaded morphology of activated and extended PRL loci (Fig. 1, supplementary material Fig. S1) with those bearing the MMTV array (Muller et al., 2001).

Table 3. Summary of PRL array size in cells transiently expressing GFP-ER and each of the GFP-ER-deletion mutants

	Vehicle	E2	4HT	ICI
GFP-ER	Decondensed	Decondensed	Condensed	Condensed
GFP-ER (1-282)	n.a.	n.a.	n.a.	n.a.
GFP-ER (1-534)	n.a.	Condensed	Condensed	Condensed
GFP-ER (1-554)	Decondensed	Decondensed	Condensed	Condensed

Cells were treated with vehicle or ligand (10 nM, 2 hours). Condensed and decondensed refers to arrays with the appearance shown in Fig. 2C,D and 2B, respectively.

n.a. indicates no accumulation of mutated GFP-ER at the PRL array.

Our results using truncated receptors show that the GFP-ER_{282} (AF1 plus the DNA-binding domain) is not detectable at the PRL array, suggesting that the DBD is not sufficient for in vivo access to native ER-response elements in a chromosomal environment. Helix-12 appears to be required, presumably for fostering productive ER-protein interactions and array decondensation. We noticed that the rate of nuclear mobility of ER appears to be directly related to the number of functional domains present. The same correlation has been noticed for receptor residency time at the PRL array. The observations that GFP-ER_{534} interacts with the array only in the presence of E2, and the array remains condensed (and presumably inactive, i.e. no RNAPII recruitment) are consistent with previous in vitro and transient transfection data on this truncated receptor. This underscores the biological relevance of the PRL array-containing cell lines for future studies of ER–Pit-1 synergistic interactions.

Collectively, the data support a stochastic model of nuclear function (Misteli, 2001; Vermeulen and Houtsmuller, 2002) because fast (and regulated) ER exhibits altered exchange rates at the chromosomally integrated PRL array. As such, these results do not necessarily support the canonical view of pre-formed, stable holo-complexes recruited to promoters as the principal mechanism of transcription regulation but rather suggest that complex formation can be highly transient in living cells, and stochastically assembled (Peterson, 2003) influenced by probabilistic interactions. Our current efforts focus on documenting the highly dynamic nature of these interactions and quantitative multiplex read-outs of NR function, particularly through high-throughput screening technologies using high resolution and automated microscopy (Perlman et al., 2004).

Materials and Methods

Prolactin Pit-1 ID-ERE concatemer and reporter constructions

We generated cell lines bearing integrated rat prolactin (PRL) promoter-enhancer that contain no viral or bacterial components (e.g. entirely mammalian regulatory elements). Advantages of PRL control elements for this purpose are: (1) they are well characterized in terms of binding and transcriptional activation by Pit-1 and ER (Barron et al., 1989; Cao et al., 1987; Crenshaw et al., 1989; Day et al., 1990; Howard and Maurer, 1995; Ingraham et al., 1990; Mangalam et al., 1989; Nelson et al., 1988; Smith et al., 1995), (2) they are responsive to 17-β estradiol (E2) through transcriptional synergy by Pit-1 and ER (Day et al., 1990; Day and Maurer, 1989; Holloway et al., 1995; Nowakowski and Maurer, 1994; Seyfred and Gorski, 1990), (3) they were useful in some of the original work to characterize transcriptional downregulation by the antiestrogen 4-hyrdroxytamoxifen (4HT) (Gothard et al., 1996; Jordan et al., 1988; Lieberman et al., 1983; Seyfred and Gorski, 1990) and, (4) alterations of their chromatin structure in response to E2 (Cullen et al., 1993; Durrin and Gorski, 1985; Durrin et al., 1984; Gothard et al., 1996; Malayer and Gorski, 1995; Maurer, 1985; Seyfred and Gorski, 1990; Willis and Seyfred, 1996) and 4HT (Gothard et al., 1996; Liu and Bagchi, 2004; Seyfred and Gorski, 1990) are well studied.

The design of the Pit-1–ERE array began with a prolactin promoter enhancer construct (pDm66/Enh) originally described by Smith et al. (Smith et al., 1995), which consists of a transcriptional fusion of a short region (–66 to +1) of the prolactin (PRL) promoter containing the transcription start site and a high-affinity Pit-1-binding site (1P, Fig. 1A) driving expression of a luciferase (Luc) reporter. Linked upstream is the native distal enhancer of prolactin (–1807 to –1498) that contains four Pit-1 binding sites, 1D, 2D, 3D and 4D (Nelson et al., 1988), and five EREs (Day et al., 1990; Day and Maurer, 1989; Holloway et al., 1995; Nowakowski and Maurer, 1994; Seyfred and Gorski, 1990), PRL1-5 (Fig. 1A). This construct was stably integrated into the chromosomes of HeLa cells (HeLa-

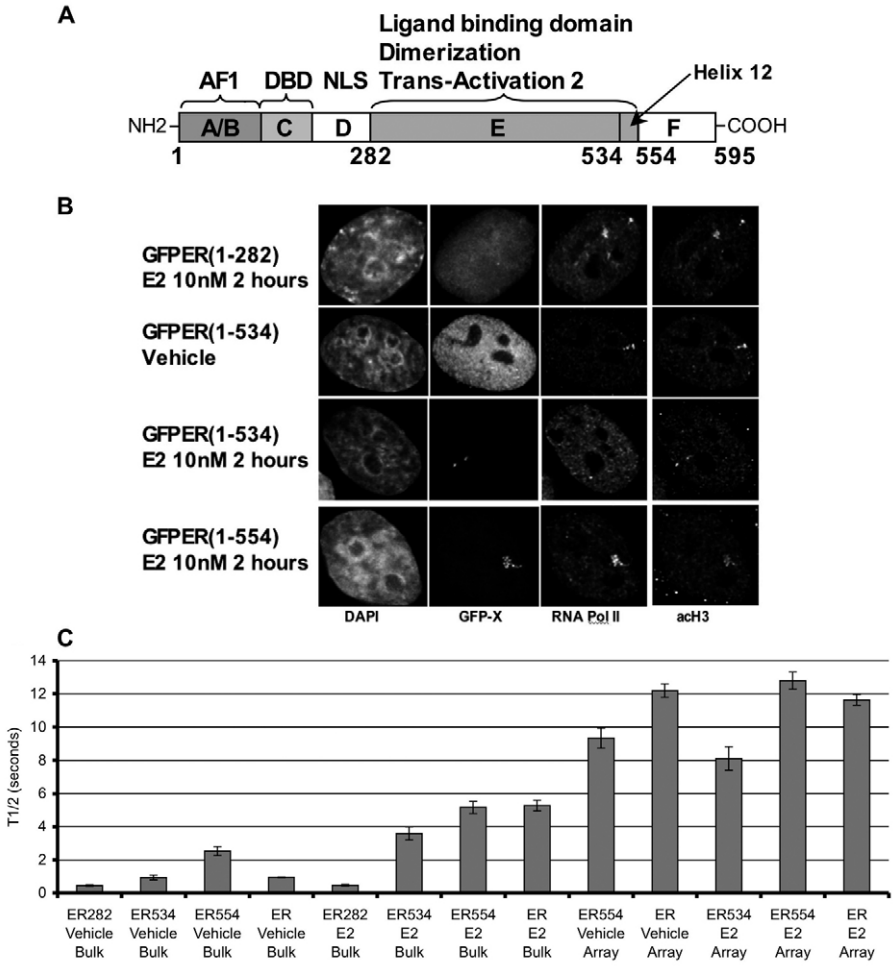

Fig. 11. ER domains required for PRL array targeting. (A) Schematic of ER functional domains with residue coordinates of the deletion mutants used in these experiments. (B) Representative images of GFP-ER_{282}, GFP-ER_{534} and GFP-ER_{554} colocalized with endogenous RNAPII or acetylated histone H3 by immunofluorescence. Each truncation was transiently expressed in PRL-HeLa cells and treated with vehicle or E2 (10 nM, 2 hrs) as indicated. GFP-X refers to the GFP signal captured from each receptor. DAPI indicates counterstained nuclei. (C) Comparison of GFP-ER and GFP-ER truncation mobility within the nucleoplasm or the array. PRL-HeLa cells were treated with vehicle or E2. Bulk denotes recovery times in the nucleoplasm and array identifies recovery times at the PRL array. Half-time of recovery was determined and is shown as a bar graph (see Materials and Methods). n=30 for FRAP analysis under each condition,

PRL-dm66-Enh, e.g. 1XPRL) and tested for Pit-1–ER synergy by transiently expressing one or both of these activators. As expected, expression of Pit-1 or ER alone results in increased levels of luciferase activity over background (seven- or fourfold, respectively, supplementary material Fig. S1B). Interestingly, ER activates this construct in the absence of Pit-1 and E2, which is consistent with GFP-ER interactions with the PRL-integrated array below. In the absence of hormone, exogenous expression of both Pit-1 and ER lead to an approximately twofold induction of luciferase activity compared with that promoted by Pit-1 alone, which increased to a fourfold induction in the presence of E2. These data are in agreement with previous experiments (Day et al., 1990; Day and Maurer, 1989; Holloway et al., 1995; Nowakowski and Maurer, 1994; Seyfred and Gorski, 1990), and indicate that this unit would serve well as an integrated reporter in HeLa cells carrying a visible array.

To construct the array-containing plasmids to establish the cell line used in this paper, we first added one unit of the ER-Pit-1 'synergy element' (Fig. 1B) onto the 5′-end of the native enhancer. This element contains one Pit-1-binding site and two EREs (1D, overlapping a full, imperfect site PRL1 and an inverted half site, PRL5, respectively). This complex-binding site (Fig. 1B) was previously shown to be cruial for the transcriptional synergy mediated by Pit-1 and ER (Nowakowski and Maurer, 1994). The relevant parts of plasmid p1X-PRLLuc, are shown schematically in Fig. 1C. In a separate cloning vector (pBS), reiterative cloning steps generated p2X, 4X, 8X, in which X refers to the number of element repeats in the array. A recombination event generated 13X and subsequent reiterative cloning generated 26X, 52X and 104X. These arrays were transferred into the PRL-Luc plasmids to test for functionality. Transient-transfection assays confirmed the qualitative functionality of three of these constructs (13X, 26X and 52X) with respect to transcription promoted by GFP–Pit-1 (supplementary material Fig. S1A). For integration into the chromosomes of HeLa cells, the Luc reporter was replaced with dsRED2-SKL fluorescent protein, which is similar to the CFP-SKL reporter protein used previously by Spector and co-workers (Tsukamoto et al., 2000). The SKL peptide represents the amino acids that target proteins to peroxisomes; in our hands, the signal of the dsRED2 reporter is much brighter than that of CFP, and allows an additional color to be used in labeling studies. Here, we describe results from analyses of one of our clonal HeLa lines (number 23) harboring the p52X-PRLdsRed2-Ser-Lys-Leu (SKL) plasmid, referred to throughout this manuscript as PRL-HeLa cells.

Table 4. Summary of photobleaching results comparing GFP-ER- and GFP-ER-truncation mutants

	Nucleoplasm vehicle				Nucleoplasm E2				Array vehicle		Array E2		
$t_{1/2}$	ER282	ER534	ER554	ER	ER282	ER534	ER554	ER	ER554	ER	ER534	ER554	ER
Mean	0.45	0.93	2.54	0.94	0.46	3.59	5.16	5.28	9.33	12.19	8.12	12.79	11.64
s.e.m.	0.06	0.13	0.27	0.02	0.05	0.40	0.37	0.32	0.60	0.40	0.72	0.52	0.33
n	10	10	10	30	10	10	10	30	20	30	10	20	30

Half-time of recovery within the nucleoplasm ($t_{1/2}$, in seconds) is shown for ER282, ER534, ER554, and ER in vehicle and E2 (10 nM) treated cells. Array associated $t_{1/2}$ is shown for ER534 (E2 treatment only), ER554 and ER (vehicle and E2 treatments).

s.e.m., standard error of the mean recovery times; n, number of cells examined.

FISH and Southern analyses of PRL-HeLa cells

DNA fluorescent in situ hybridization (FISH) confirmed the integration of the transgene array (e.g. PRL array) that showed an intranuclear focus of signal (Fig. 2B). Colocalization of GFP-ER–Pit1 with DNA-FISH and RNA-FISH focus signals also confirmed the integration of the promoter array and demonstrated protein-DNA interaction and transcriptional activity, respectively (Fig. 2B). Quantitative Southern blotting indicated approximately 200-300 copies of p52X-PRL-dsRED2skl integrated into the HeLa genome (data not shown). These data indicate that the p52X-PRL-dsRed2-SKL-hygro vector integrated into the HeLa genome at a specific locus to form a promoter array that is transcriptionally active and visible through interaction with GFP-ER and/or GFP-Pit-1.

ER and Pit-1 interact with the PRL array separately

To determine whether GFP-ER or GFP-Pit-1 individually interact with the PRL array, single transfections of PRL-HeLa cells were performed. These experiments, originally carried out in OptiMEM (growth-factor-containing minimal essential medium) containing charcoal-stripped serum, showed both GFP-ER and GFP-Pit-1 can target the array individually. To properly assess ligand (ER) or growth factor (Pit-1) stimulation, we grew cells for a minimum of 48 hours in hormone-free stripped and dialyzed serum and DMEM (Dulbecco's modified Eagle's medium). Quantitative examination of the number of cells expressing Pit-1 alone (GFP-tagged or untagged) indicated inefficient targeting to the array under hormone-free conditions (data not shown). These data suggest an influence of cell signaling pathways on GFP-Pit-1 interactions with the PRL array, which is consistent with previously reported Pit-1 transcription assays (Xu et al., 1998).

In contrast to GFP-Pit-1, GFP-ER was capable of targeting the arrays in ~75% of the cells in hormone-free medium. Interestingly, E2-treatment (2 hours at 10^{-8} M; a time and ligand concentration used throughout these studies) resulted in virtually all transfected cells demonstrating targeted arrays by GFP-ER (Fig. 2C). Consistent with our observations in the screens above, when CFP-Pit-1 was co-expressed with YFP-ER in PRL-HeLa cells cultured in hormone-free medium or in OptiMEM with serum, Pit-1 was found to target together with ER at the array (Fig. 2). Thus, in this system, under conditions of minimal global cell signaling, the data indicate that Pit-1 and ER can simultaneously interact with array chromatin. In the experiments reported below, we concentrated on ligand-dependent observations of ER at the array.

Immunolabeling

Antibody labeling was performed as described previously (Stenoien et al., 2000) using 4% formaldehyde fixation (30 minutes) and indirect labeling with Alexa Fluor-488, -546 or -633 (Molecular Probes) conjugated secondary antibodies. Since the majority of antibodies had previously been mapped to the nuclear compartment, we were able to perform localization experiments without confusing the well-defined dsRED2skl peroxisome signal with antibody label, even when using secondary antibodies with overlapping spectra. DAPI (1 μg/ml) was used to label DNA prior to mounting in Slow Fade (Molecular Probes). Affinity-purified rabbit antibodies against SRC-1 and SRC-3 were a kind gift of Jeimin Wong (Baylor College of Medicine, Houston, TX); cyclin T, cdk9, BRG-1, RNAPII large subunit, acetylated histone H3 and dimethylated histone H3 (K4 and K9) were obtained from Abcam or Upstate Biotechnology and all used at 1 μg/ml for 1 hour at room temperature or overnight at 4°C.

Fluorescent in situ hybridization (FISH)

The methods used here, including procedures for non-isotopic probe preparation and fluorescent in situ hybridization, have been published in detail elsewhere (Johnson et al., 1991; Tam et al., 2002). Briefly, coverslips with adherent cells were rinsed twice in PBS, dipped in cytoskeleton (CSK) buffer (100 mM NaCl, 300 mM sucrose, 3 mM MgCl2, 10 mM PIPES pH 6.8) (Fey et al., 1986), extracted on ice for 5 minutes in CSK buffer containing 0.5% Triton X-100 and 2 mM vanadyl-ribonucleoside complex (VRC; Gibco-BRL), rinsed in CSK-VRC buffer, fixed in 4% paraformaldehyde with PBS for 10 minutes, rinsed again in PBS and stored in 0.4% paraformaldehyde at 4°C until use.

Probes substituted with biotin-labeled deoxynucleotides were made by modifications of standard nick-translation procedures (Tam et al., 2002). For hybridization to DNA, cells were first denatured by incubation in 0.07 M NaOH, 70% EtOH for 5 minutes. This incubation denatures the DNA prior to hybridization and removes RNA. RNA hybridization refers to samples in which the cellular DNA was not heat-denatured, leaving it inaccessible for hybridization. Hybridization to RNA or DNA was carried out overnight at 37°C in rehydration buffer (2 mM VRC, 2 mg/ml BSA, 0.05 g/ml Dextran, and 2× SSC) containing 5 μg/ml probe and 50% formamide. After incubation, samples were rinsed in a dilution series of NaCl–Na-citrate (SSC) buffers, analysed for biotin using streptavidin-conjugated Alexa Fluor-594 (Molecular Probes, Eugene, OR) and rinsed in a dilution series of PBS. Where indicated, cells were counter-stained with 1 mg/ml DAPI (Sigma, St Louis, MO). Coverslips were then mounted on slides in Vectashield (Vector Laboratories, Burlingame, CA).

To quantify FISH signals, a 20 plane 128×128 (pixels), 0.2 μm *Z*-stack was collected (constant 100-millisecond exposure). A circular region containing the array was selected and a region of the same size was used to select the background nucleoplasm. Total array associated FISH signal was determined by quantifying the cumulative intensity of the array region after sum projection and background subtraction.

Fixed-cell- and time-lapse-imaging

XFP-fusions and immunofluorescently labeled cells were imaged using a DeltaVision Restoration Microscopy system (Applied Precision, Issaqua, WA) and applying a constrained iterative deconvolution process. Whole nuclear volumes were collected at 0.2 μm *Z*-steps, and images from select focal planes or 3D-projections were imported into Adobe PhotoShop. Histogram adjustments were made relevant to negative controls, which routinely included non-transfected cells and/or omission of primary antibodies. Live imaging was performed by collecting short *Z*-stacks (~5-10 focal planes at 300-nm increments); neutral density for the green channel was set at 50% and the images were binned 2×2. Typical exposures were for <1 second, and time points from 3-10 minutes per stack. Projected images from each time point were used to create a QuickTime movie.

Live cell imaging

Cells were grown in 35-mm Delta T dishes (Bioptechs) and secured to a stage adapter for temperature control. HEPES-buffered media was gassed overnight in a 5% CO_2 incubator, and circulated through the Delta T dish using a Bioptechs peristaltic pump and inflow-outflow tubing. The temperature was controlled to 37°C (± ~0.1 degree); a Bioptechs objective-heating collar was also used (also 37°C). The Delta T dish was covered with a black plastic lid, with room for input-output tubing. For time-lapse imaging, a 63× objective (NA=1.4) was used.

Photobleaching parameters and calculations

For imaging, PRL-HeLa cells were plated and transfected in Delta T dishes. Live cell microscopy was performed using a Zeiss 510 confocal microscope using the 488-nm laser line of the argon laser at 75% of maximal power. In all experiments cells were maintained at 37°C and fresh media containing the appropriate ligand was cycled over the cells. All imaging was done with a 63× objective (NA=1.4) with pinhole set at either 4 Airy units (Au) (FRAP and $FRAP_{intra\text{-}array}$) or 10 Au (i-FRAP). Scanning was bidirectional at the highest possible rate using a 3.5× zoom with laser power attenuated to 1% of bleach intensity. For all experiments, cells were selected for low levels of GFP-ER expression to limit experimental artifacts. For FRAP experiments, a single pre-bleach image was acquired followed by ten iterative bleach pulses of a total duration of 530 milliseconds using a circular bleach region of interest (ROI) of the diameter of either 32 pixels for large arrays or 18 pixels for small arrays. Single-section images were collected every 250 milliseconds for 60 seconds. Relative fluorescence signal in the bleached region was determined by two sequential normalization steps using the mean ROI (I_t) bleach signals and the mean nucleus bleach signals (N_t):

$$(1)\quad V = \frac{(I_t/N_t)}{(I_{prebleach}/N_{prebleach})} \qquad (2)\quad \frac{(V_t - V_{min})}{(V_{max} - V_{min})}\ .$$

Pre-bleach values are not used in the second normalization step. Half-time of maximal recovery was determined by fitting a logarithmic equation to the recovery curve and determining the value of t when y=0.5 using the Excel curve-fitting function. Inverse-FRAP (i-FRAP) experiments were performed in a similar manner except that three iterative bleach pulses were used for the total duration of 600 milliseconds, with a bleach ROI containing the whole nucleus, excluding the array. Relative fluorescence and half-time of loss were also determined in a similar manner except pre-bleach values were retained.

For $FRAP_{intra\text{-}array}$ experiments, five pre-bleach images were collected followed by a single bleach pulse of 220 milliseconds using a circular bleach ROI of the diameter of 13 pixels. Single-section images were collected every 500 milliseconds for 75 seconds. The relative fluorescence signal in the bleached region was determined as above. The unbinding-rate constant and half-time of recovery was calculated by fitting a single-term exponential equation ($1–e^{-kt}$) to the recovery curve (see Lele et al., 2004 for detailed methods).

Quantitative image analyses by HTM

PRL-HeLa cells transiently expressing GFP-ER were treated with 10 nM E2, 4HT, or ICI for two hours, fixed and DAPI-stained. Cells were imaged using the Cell Lab IC 100 Image Cytometer (Beckman Coulter) with a Nikon 40× Plan S Fluor 0.90 NA objective. Two channels were imaged: channel 0 (DAPI) was used to find the focus and nuclei and channel 1 was used to image GFP-ER. A proprietary algorithm (GPCR) developed at Beckman Coulter was used to identify and quantify the GFP-ER targeted PRL array. The parameters for the GPCR algorithm were: object scale = 30 and minimum peak-height = 10. Foci identified by the GPCR algorithm are masked. The area of the mask in pixels is the measure of PRL array size. Channel 1 was offset 2 microns from the DAPI focus for cells in all treatment conditions. This offset provided the greatest number of in focus arrays identified by the GPCR algorithm. After image acquisition and application of the GPCR algorithm the total cell populations for each treatment were progressively filtered (gated) using the

same criteria. Nuclei clusters, mitotic cells and apoptotic cells were filtered from the total cell population using an intersection of DNA-content and DNA-cluster gates. In addition, low GFP-ER–expression gates and low aggregate-number-gates were generated and applied to produce the final cell population to be analyzed. From the final population of cells, the array size was determined using the GPCR mask. The images and masks were visually inspected for accuracy. Unpaired Student's *t*-tests assuming equal variance were performed to determine statistical significance (two-tailed, $P<0.05$).

The authors wish to thank Ann Nye-Carpenter, who provided early guidance in the establishment of the cell lines, and J. H. Price (Burnham Institute and Vala Sciences, San Diego, CA) for invaluable help with the automated image cytometry. We also thank B. W. O'Malley, J. A. Nickerson, J. Lawrence's laboratory, and the anonymous reviewers of the manuscript for many helpful suggestions. This work was supported from NIH grants DK55622 (M.A.M.), DOD W81XWH-04-1-0700 (Z.D.S.) and NASA NN A04CC96G (D.E.I.). All imaging was performed in the Department of Molecular and Cellular Biology Integrated Microscopy Core, supported by HD-07495 (Center for Reproductive Biology, B. W. O'Malley), NCI-CA64255 (Hormonal Regulation of Breast Cancer PPG, D. Medina) and departmental funds. C.H. and A.S. were supported in part by training grants in Reproductive Biology (DK12345) and Pharamoinformatics (GM12345), respectively.

References

Barron, E. A., Cao, Z., Schneider, B. G., Kraig, E., Carrillo, A. J. and Sharp, Z. D. (1989). Dual functions of a cis-acting element within the rat prolactin gene promoter. *Mol. Cell. Biol.* **9**, 817-819.

Becker, M., Baumann, C., John, S., Walker, D. A., Vigneron, M., McNally, J. G. and Hager, G. L. (2002). Dynamic behavior of transcription factors on a natural promoter in living cells. *EMBO Rep.* **3**, 1188-1194.

Bosisio, D., Marazzi, I., Agresti, A., Shimizu, N., Bianchi, M. E. and Natoli, G. (2006). A hyper-dynamic equilibrium between promoter-bound and nucleoplasmic dimers controls NF-kappaB-dependent gene activity. *EMBO J.* **25**, 798-810.

Cao, Z. D., Barron, E. A., Carillo, A. J. and Sharp, Z. D. (1987). Reconstitution of cell-type-specific transcription of the rat prolactin gene in vitro. *Mol. Cell. Biol.* **7**, 3402-3408.

Carrillo, A. J., Sharp, Z. D. and DePaolo, L. V. (1987). Correlation of rat pituitary prolactin messenger ribonucleic acid and hormone content with serum levels during the estrogen-induced surge. *Endocrinology* **121**, 1993-1999.

Coleman, K. M. and Smith, C. L. (2001). Intracellular signaling pathways: nongenomic actions of estrogens and ligand-independent activation of estrogen receptors. *Front. Biosci.* **6**, D1379-D1391.

Crenshaw, E. B., 3rd, Kalla, K., Simmons, D. M., Swanson, L. W. and Rosenfeld, M. G. (1989). Cell-specific expression of the prolactin gene in transgenic mice is controlled by synergistic interactions between promoter and enhancer elements. *Genes Dev.* **3**, 959-972.

Cullen, K. E., Kladde, M. P. and Seyfred, M. A. (1993). Interaction between transcription regulatory regions of prolactin chromatin. *Science* **261**, 203-206.

Day, R. N. and Maurer, R. A. (1989). The distal enhancer region of the rat prolactin gene contains elements conferring response to multiple hormones. *Mol. Endocrinol.* **3**, 3-9.

Day, R. N., Koike, S., Sakai, M., Muramatsu, M. and Maurer, R. A. (1990). Both Pit-1 and the estrogen receptor are required for estrogen responsiveness of the rat prolactin gene. *Mol. Endocrinol.* **4**, 1964-1971.

Dundr, M., Hoffmann-Rohrer, U., Hu, Q., Grummt, I., Rothblum, L. I., Phair, R. D. and Misteli, T. (2002). A kinetic framework for a mammalian RNA polymerase in vivo. *Science* **298**, 1623-1626.

Durrin, L. K. and Gorski, J. (1985). The prolactin gene hypersensitive sites are present early in development and are not induced by estrogen administration. *Endocrinology* **117**, 2098-2105.

Durrin, L. K., Weber, J. L. and Gorski, J. (1984). Chromatin structure, transcription, and methylation of the prolactin gene domain in pituitary tumors of Fischer 344 rats. *J. Biol. Chem.* **259**, 7086-7093.

Fey, E. G., Ornelles, D. A. and Penman, S. (1986). Association of RNA with the cytoskeleton and the nuclear matrix. *J. Cell Sci. Suppl.* **5**, 99-119.

Gothard, L. Q., Hibbard, J. C. and Seyfred, M. A. (1996). Estrogen-mediated induction of rat prolactin gene transcription requires the formation of a chromatin loop between the distal enhancer and proximal promoter regions. *Mol. Endocrinol.* **10**, 185-195.

Holloway, J. M., Szeto, D. P., Scully, K. M., Glass, C. K. and Rosenfeld, M. G. (1995). Pit-1 binding to specific DNA sites as a monomer or dimer determines gene-specific use of a tyrosine-dependent synergy domain. *Genes Dev.* **9**, 1992-2006.

Howard, P. W. and Maurer, R. A. (1995). A composite Ets/Pit-1 binding site in the prolactin gene can mediate transcriptional responses to multiple signal transduction pathways. *J. Biol. Chem.* **270**, 20930-20936.

Htun, H., Holth, L. T., Walker, D., Davie, J. R. and Hager, G. L. (1999). Direct visualization of the human estrogen receptor alpha reveals a role for ligand in the nuclear distribution of the receptor. *Mol. Biol. Cell* **10**, 471-486.

Ingraham, H. A., Flynn, S. E., Voss, J. W., Albert, V. R., Kapiloff, M. S., Wilson, L. and Rosenfeld, M. G. (1990). The POU-specific domain of Pit-1 is essential for sequence-specific, high affinity DNA binding and DNA-dependent Pit-1-Pit-1 interactions. *Cell* **61**, 1021-1033.

Janicki, S. M., Tsukamoto, T., Salghetti, S. E., Tansey, W. P., Sachidanandam, R., Prasanth, K. V., Ried, T., Shav-Tal, Y., Bertrand, E., Singer, R. H. et al. (2004). From silencing to gene expression; real-time analysis in single cells. *Cell* **116**, 683-698.

Johnson, C. V., Singer, R. H. and Lawrence, J. B. (1991). Fluorescent detection of nuclear RNA and DNA: implications for genome organization. *Methods Cell Biol.* **35**, 73-99.

Jordan, V. C., Koch, R., Langan, S. and McCague, R. (1988). Ligand interaction at the estrogen receptor to program antiestrogen action: a study with nonsteroidal compounds in vitro. *Endocrinology* **122**, 1449-1454.

Kim, M. Y., Hsiao, S. J. and Kraus, W. L. (2001). A role for coactivators and histone acetylation in estrogen receptor alpha-mediated transcription initiation. *EMBO J.* **20**, 6084-6094.

Kouzarides, T. (2002). Histone methylation in transcriptional control. *Curr. Opin. Genet. Dev.* **12**, 198-209.

Lele, T., Oh, P., Nickerson, J. A. and Ingber, D. E. (2004). An improved mathematical model for determination of molecular kinetics in living cells with FRAP. *Mech. Chem. Biosyst.* **1**, 181-190.

Lieberman, M. E., Jordan, V. C., Fritsch, M., Santos, M. A. and Gorski, J. (1983). Direct and reversible inhibition of estradiol-stimulated prolactin synthesis by antiestrogens in vitro. *J. Biol. Chem.* **258**, 4734-4740.

Liu, X. F. and Bagchi, M. K. (2004). Recruitment of distinct chromatin-modifying complexes by tamoxifen-complexed estrogen receptor at natural target gene promoters in vivo. *J. Biol. Chem.* **279**, 15050-15058.

Malayer, J. R. and Gorski, J. (1995). The role of estrogen receptor in modulation of chromatin conformation in the 5′ flanking region of the rat prolactin gene. *Mol. Cell. Endocrinol.* **113**, 145-154.

Mangalam, H. J., Albert, V. R., Ingraham, H. A., Kapiloff, M., Wilson, L., Nelson, C., Elsholtz, H. and Rosenfeld, M. G. (1989). A pituitary POU domain protein, Pit-1, activates both growth hormone and prolactin promoters transcriptionally. *Genes Dev.* **3**, 946-958.

Maurer, R. A. (1985). Selective binding of the estradiol receptor to a region at least one kilobase upstream from the rat prolactin gene. *DNA* **4**, 1-9.

McKenna, N. J., Lanz, R. B. and O'Malley, B. W. (1999). Nuclear receptor coregulators: cellular and molecular biology. *Endocr. Rev.* **20**, 321-344.

McNally, J. G., Muller, W. G., Walker, D., Wolford, R. and Hager, G. L. (2000). The glucocorticoid receptor: rapid exchange with regulatory sites in living cells. *Science* **287**, 1262-1265.

Metivier, R., Penot, G., Hubner, M. R., Reid, G., Brand, H., Kos, M. and Gannon, F. (2003). Estrogen receptor-α directs ordered, cyclical, and combinatorial recruitment of cofactors on a natural target promoter. *Cell* **115**, 751-763.

Misteli, T. (2001). Protein dynamics: implications for nuclear architecture and gene expression. *Science* **291**, 843-847.

Muller, W. G., Walker, D., Hager, G. L. and McNally, J. G. (2001). Large-scale chromatin decondensation and recondensation regulated by transcription from a natural promoter. *J. Cell Biol.* **154**, 33-48.

Nelson, C., Albert, V. R., Elsholtz, H. P., Lu, L. I. and Rosenfeld, M. G. (1988). Activation of cell-specific expression of rat growth hormone and prolactin genes by a common transcription factor. *Science* **239**, 1400-1405.

Nowakowski, B. E. and Maurer, R. A. (1994). Multiple Pit-1-binding sites facilitate estrogen responsiveness of the prolactin gene. *Mol. Endocrinol.* **8**, 1742-1749.

Nye, A. C., Rajendran, R. R., Stenoien, D. L., Mancini, M. A., Katzenellenbogen, B. S. and Belmont, A. S. (2002). Alteration of large-scale chromatin structure by estrogen receptor. *Mol. Cell. Biol.* **22**, 3437-3449.

Pakdel, F., Le Goff, P. and Katzenellenbogen, B. S. (1993). An assessment of the role of domain F and PEST sequences in estrogen receptor half-life and bioactivity. *J. Steroid Biochem. Mol. Biol.* **46**, 663-672.

Perlman, Z. E., Slack, M. D., Feng, Y., Mitchison, T. J., Wu, L. F. and Altschuler, S. J. (2004). Multidimensional drug profiling by automated microscopy. *Science* **306**, 1194-1198.

Peterson, C. L. (2003). Transcriptional activation: getting a grip on condensed chromatin. *Curr. Biol.* **13**, R195-R197.

Reid, G., Hubner, M. R., Metivier, R., Brand, H., Denger, S., Manu, D., Beaudouin, J., Ellenberg, J. and Gannon, F. (2003). Cyclic, proteasome-mediated turnover of unliganded and liganded ERalpha on responsive promoters is an integral feature of estrogen signaling. *Mol. Cell* **11**, 695-707.

Robinett, C. C., Straight, A., Li, G., Willhelm, C., Sudlow, G., Murray, A. and Belmont, A. S. (1996). In vivo localization of DNA sequences and visualization of large-scale chromatin organization using lac operator/repressor recognition. *J. Cell Biol.* **135**, 1685-1700.

Seyfred, M. A. and Gorski, J. (1990). An interaction between the 5′ flanking distal and proximal regulatory domains of the rat prolactin gene is required for transcriptional activation by estrogens. *Mol. Endocrinol.* **4**, 1226-1234.

Shang, Y., Hu, X., DiRenzo, J., Lazar, M. A. and Brown, M. (2000). Cofactor dynamics and sufficiency in estrogen receptor-regulated transcription. *Cell* **103**, 843-852.

Smith, K. P., Liu, B., Scott, C. and Sharp, Z. D. (1995). Pit-1 exhibits a unique promoter spacing requirement for activation and synergism. *J. Biol. Chem.* **270**, 4484-4491.

Stenoien, D. L., Mancini, M. G., Patel, K., Allegretto, E. A., Smith, C. L. and Mancini, M. A. (2000). Subnuclear trafficking of estrogen receptor-α and steroid receptor coactivator-1. *Mol. Endocrinol.* **14**, 518-534.

Stenoien, D. L., Nye, A. C., Mancini, M. G., Patel, K., Dutertre, M., O'Malley, B. W., Smith, C. L., Belmont, A. S. and Mancini, M. A. (2001a). Ligand-mediated assembly and real-time cellular dynamics of estrogen receptor α-coactivator complexes in living cells. *Mol. Cell. Biol.* **21**, 4404-4412.

Stenoien, D. L., Patel, K., Mancini, M. G., Dutertre, M., Smith, C. L., O'Malley, B. W. and Mancini, M. A. (2001b). FRAP reveals that mobility of oestrogen receptor-α is ligand- and proteasome-dependent. *Nat. Cell Biol.* **3**, 15-23.

Tam, R., Johnson, C., Shopland, L., McNeil, J. and Lawrence, J. B. (2002). Applications of RNA FISH for visualizing gene expression and nuclear architecture. In *FISH* (ed. B. G. Beatty, S. Mai and J. A. Squire), pp. 93-118. Oxford: Oxford University Press.

Tsukamoto, T., Hashiguchi, N., Janicki, S. M., Tumbar, T., Belmont, A. S. and Spector, D. L. (2000). Visualization of gene activity in living cells. *Nat. Cell Biol.* **2**, 871-878.

Tulin, A. and Spradling, A. (2003). Chromatin loosening by poly(ADP)-ribose polymerase (PARP) at Drosophila puff loci. *Science* **299**, 560-562.

Tumbar, T., Sudlow, G. and Belmont, A. S. (1999). Large-scale chromatin unfolding and remodeling induced by VP16 acidic activation domain. *J. Cell Biol.* **145**, 1341-1354.

Tzukerman, M. T., Esty, A., Santiso-Mere, D., Danielian, P., Parker, M. G., Stein, R. B., Pike, J. W. and McDonnell, D. P. (1994). Human estrogen receptor transactivational capacity is determined by both cellular and promoter context and mediated by two functionally distinct intramolecular regions. *Mol. Endocrinol.* **8**, 21-30.

Vermeulen, W. and Houtsmuller, A. B. (2002). The transcription cycle in vivo. A blind watchmaker at work. *Mol. Cell* **10**, 1264-1266.

Willis, S. D. and Seyfred, M. A. (1996). Pituitary-specific chromatin structure of the rat prolactin distal enhancer element. *Nucleic Acids Res.* **24**, 1065-1072.

Xu, L., Lavinsky, R. M., Dasen, J. S., Flynn, S. E., McInerney, E. M., Mullen, T. M., Heinzel, T., Szeto, D., Korzus, E., Kurokawa, R. et al. (1998). Signal-specific co-activator domain requirements for Pit-1 activation. *Nature* **395**, 301-306.